DNA-dependent binding of nargenicin to DnaE1 inhibits replication in Mycobacterium tuberculosis

Chengalroyen, M.D.; Mason, M.K.; Borsellini, A.; Tassoni, R.; Abrahams, G.L.; Lynch, S.; ... ; Mizrahi, V.

ACS Infectious Diseases

pubs.acs.org/journal/aidcbc

Article

DNA-Dependent Binding of Nargenicin to DnaE1 Inhibits Replication in *Mycobacterium tuberculosis*

Melissa D. Chengalroyen,[▽] Mandy K. Mason,[▽] Alessandro Borsellini, Raffaella Tassoni, Garth L. Abrahams, Sasha Lynch, Yong-Mo Ahn, Jon Ambler, Katherine Young, Brendan M. Crowley, David B. Olsen, Digby F. Warner, Clifton E. Barry III, Helena I. M. Boshoff, Meindert H. Lamers,* and Valerie Mizrahi*

Cite This: *ACS Infect. Dis.* 2022, 8, 612−625

Read Online

ACCESS | Metrics & More | Article Recommendations | Supporting Information

ABSTRACT: Natural products provide a rich source of potential antimicrobials for treating infectious diseases for which drug resistance has emerged. Foremost among these diseases is tuberculosis. Assessment of the antimycobacterial activity of nargenicin, a natural product that targets the replicative DNA polymerase of *Staphylococcus aureus*, revealed that it is a bactericidal genotoxin that induces a DNA damage response in *Mycobacterium tuberculosis* (*Mtb*) and inhibits growth by blocking the replicative DNA polymerase, DnaE1. Cryo-electron microscopy revealed that binding of nargenicin to *Mtb* DnaE1 requires the DNA substrate such that nargenicin is wedged between the terminal base pair and the polymerase and occupies the position of both the incoming nucleotide and templating base. Comparative analysis across three bacterial species suggests that the activity of nargenicin is partly attributable to the DNA binding affinity of the replicative polymerase. This work has laid the foundation for target-led drug discovery efforts focused on *Mtb* DnaE1.

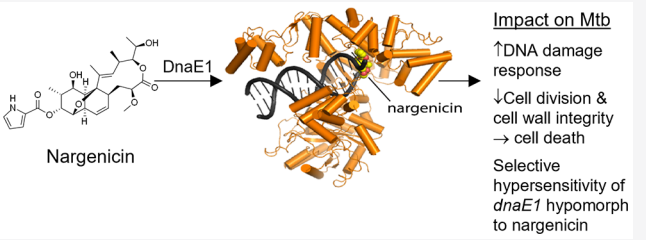

KEYWORDS: *antimicrobial drug discovery, Mycobacterium tuberculosis, DnaE1, DNA damage, DNA polymerase, nargenicin*

Claiming an estimated 1.5 million lives in 2020, tuberculosis (TB) remains one of the leading causes of death globally from an infectious disease.[1] The severe disruptions to health services wrought by the COVID-19 pandemic are predicted to worsen this grim toll by a further 1 million TB deaths per annum over the next four years.[1] In the absence of a highly efficacious vaccine, prolonged chemotherapy with combinations of anti-TB drugs forms the cornerstone of TB control. However, the increase of drug resistance through ongoing evolution and spread of drug-resistant strains of the etiologic agent, *Mycobacterium tuberculosis* (*Mtb*), is undermining current efforts. This problem, exacerbated by additional treatment delays caused by the pandemic, underscores the urgent need for new TB drugs with distinct mechanisms of action for inclusion in shorter, safer, and more effective drug regimens. The TB drug discovery and development pipeline established in recent years has begun to deliver new and repurposed drugs and combinations that have revolutionized the treatment of drug-resistant TB[2] and demonstrated that treatment shortening is an achievable goal.[3] However, maintaining this momentum requires replenishment of the pipeline with high-quality hit compounds that show mechanistic novelty.[4] This is a key objective of the Tuberculosis Drug Accelerator (TBDA).[5]

Of the vital cellular processes targeted by TB drugs in clinical use, DNA replication stands out as relatively underrepresented;[6−8] this is despite the high vulnerability of some genes essential for DNA replication in *Mtb*,[9] including those encoding DNA gyrase, the target of the fluoroquinolones, moxifloxacin, gatifloxacin, and levofloxacin, and the only DNA metabolic enzyme currently targeted for TB therapy. Fluoroquinolones inhibit DNA gyrase with bactericidal consequences for *Mtb*[10,11] and have been incorporated in second-line therapy for multidrug-resistant (MDR) TB[12] and in treatment-shortening regimens for drug-susceptible TB.[3] The identification of novel scaffolds that target DNA gyrase remains an active area of investigation,[13,14] while topoisomerase I is also being pursued as a new TB drug target.[15] Recently, the replisome—the macromolecular machine that copies the bacterial chromosome—has emerged as an attractive target for TB[6,7] and antibacterial drug discovery, more generally.[16] Key discoveries involving natural products have added impetus to exploring this target further: first, griselimycin, a cyclic depsipeptide discovered more than 50 years ago, was shown

Received: December 9, 2021
Published: February 10, 2022

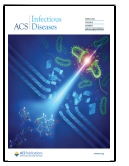

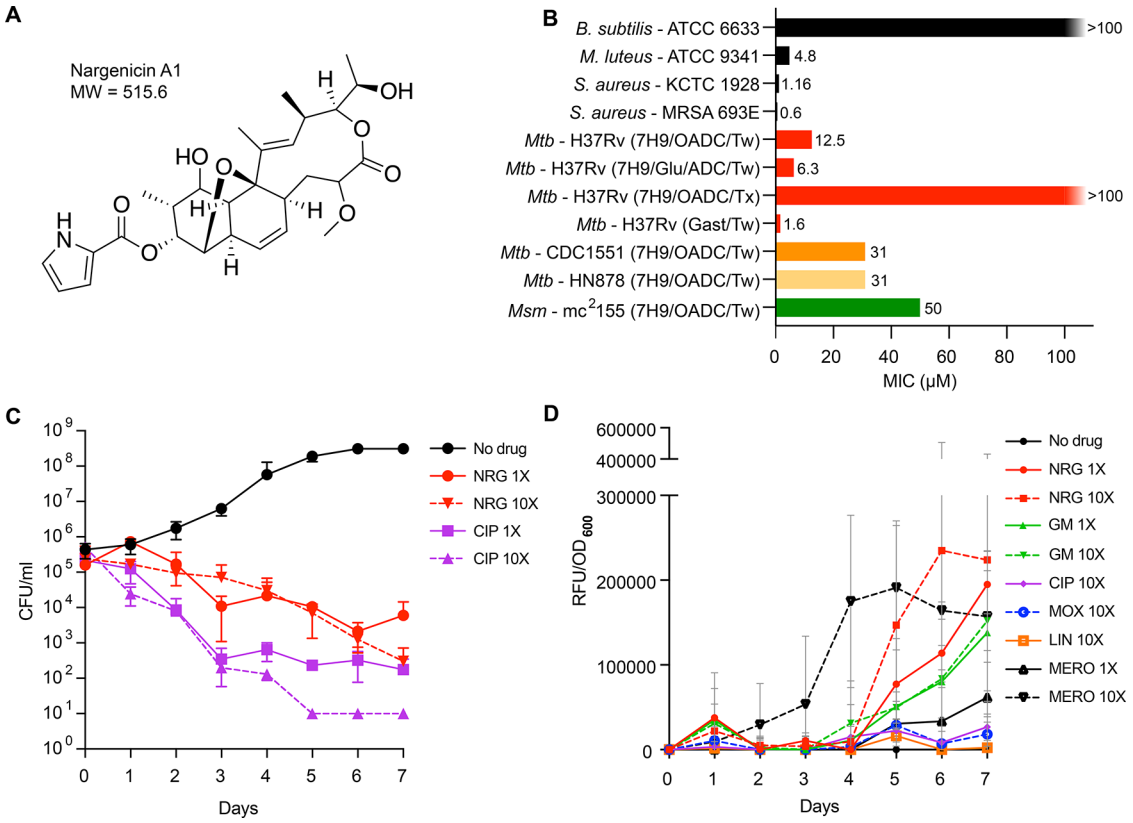

Figure 1. Antimycobacterial activity profile of nargenicin. (A) Chemical structure of nargenicin A1. (B) Antibacterial activity (minimal inhibitory concentration, MIC) of nargenicin (NRG) in mycobacteria and other organisms illustrating the effect of media composition on activity. 7H9, Middlebrook 7H9 media; GAST/(Fe), glycerol-alanine-salts (with iron); Glu, glucose; (O)ADC, (oleic acid)-albumin-dextrose-catalase; Tw, Tween-80; Tx, Tyloxapol. (C) Time−kill kinetics of nargenicin in *Mtb*, measured by CFU enumeration. Error bars represent the SD derived from two biological replicates. Ciprofloxacin (CIP; MIC = 1.5 μM) was used as a comparator. (D) Drug-induced lytic activity measured by the release of GFP from *Mtb* H37Rv-GFP at the indicated concentrations.[32] Linezolid (LIN; MIC = 1.5 μM) and meropenem (MERO; MIC = 5.2 μM) were used as the nonlytic and lytic controls, respectively. Data are representative of the two biological replicates.

to bind with high affinity and selectivity to the β-clamp (DnaN) at the site of interaction with DNA polymerase and other DNA metabolizing enzymes.[17] During DNA replication, the β-clamp interacts with DnaE1, the replicative DNA polymerase termed variously as DnaE, DnaE1, or PolC in different bacteria, greatly enhancing the processivity of the polymerase. Griselimycin interferes with the protein interaction between DnaE1 and the β-clamp, affecting the processivity of DNA replication.[17] The mechanistic novelty of griselimycin led to the development of the analogue, cyclohexyl-griselimycin, which has improved potency and stability and demonstrated comparable efficacy to rifampicin when used in combination with first-line drugs in a mouse infection model.[17] Second, studies in *Staphylococcus aureus* identified the replicative DNA polymerase, DnaE, as the target of nargenicin A1 (referred to here as nargenicin),[18] which belongs to a class of partially saturated alicyclic polyketides comprising an octalin ring (Figure 1A).[19] Nargenicin is an ether-bridged macrolide antibiotic first isolated from various *Nocardia* species almost three decades ago.[20,21] It is a narrow-spectrum antimicrobial[18] with activity against gram-positive bacteria, including methicillin-resistant *S. aureus* and *Micrococcus luteus*.[22] The identification of *narR/ngnU*,[21,23] a *dnaE* homologue immediately adjacent to the nargenicin biosynthetic gene cluster in the producer organism, *Nocardia* sp. CS682,[24] suggested a mechanism of self-resistance to nargenicin using NarR/NgnU as a "decoy".[21]

The potent bactericidal activity and low frequency of resistance for nargenicin in *S. aureus*[18] led us to investigate the antimycobacterial properties of this molecule[25] under the auspices of the TBDA. Here, we show that nargenicin is a bactericidal genotoxin that induces a DNA damage response in *Mtb* that is accompanied by cellular elongation and potential weakening of the cell envelope. We further demonstrate that the antimycobacterial activity of nargenicin is mediated through the inhibition of DNA synthesis, consistent with the inhibition of the DNA polymerase activity of purified DnaE1. Structural analysis by cryo-electron microscopy (cryo-EM) revealed a unique mode of binding by nargenicin to *Mtb* DnaE1 in the presence of DNA in which nargenicin occupies the position of both the incoming nucleotide and templating base and stacks onto the terminal base pair. We show that the antibacterial efficacy of nargenicin as a DNA replication inhibitor is attributable, at least in part, to the DNA binding affinity of the organism's replicative polymerase.

RESULTS

Nargenicin is Bactericidal against *Mtb In Vitro*. Nargenicin was shown to have a minimum inhibitory concentration (MIC) of 12.5 μM against *Mtb* H37Rv under standard culture conditions (7H9/OADC/Tw) (Figure 1B; Table S1). In this culture medium, nargenicin showed comparable activity against a range of drug-sensitive and drug-resistant clinical isolates of *Mtb* and was active against

https://doi.org/10.1021/acsinfecdis.1c00643
ACS Infect. Dis. 2022, 8, 612−625

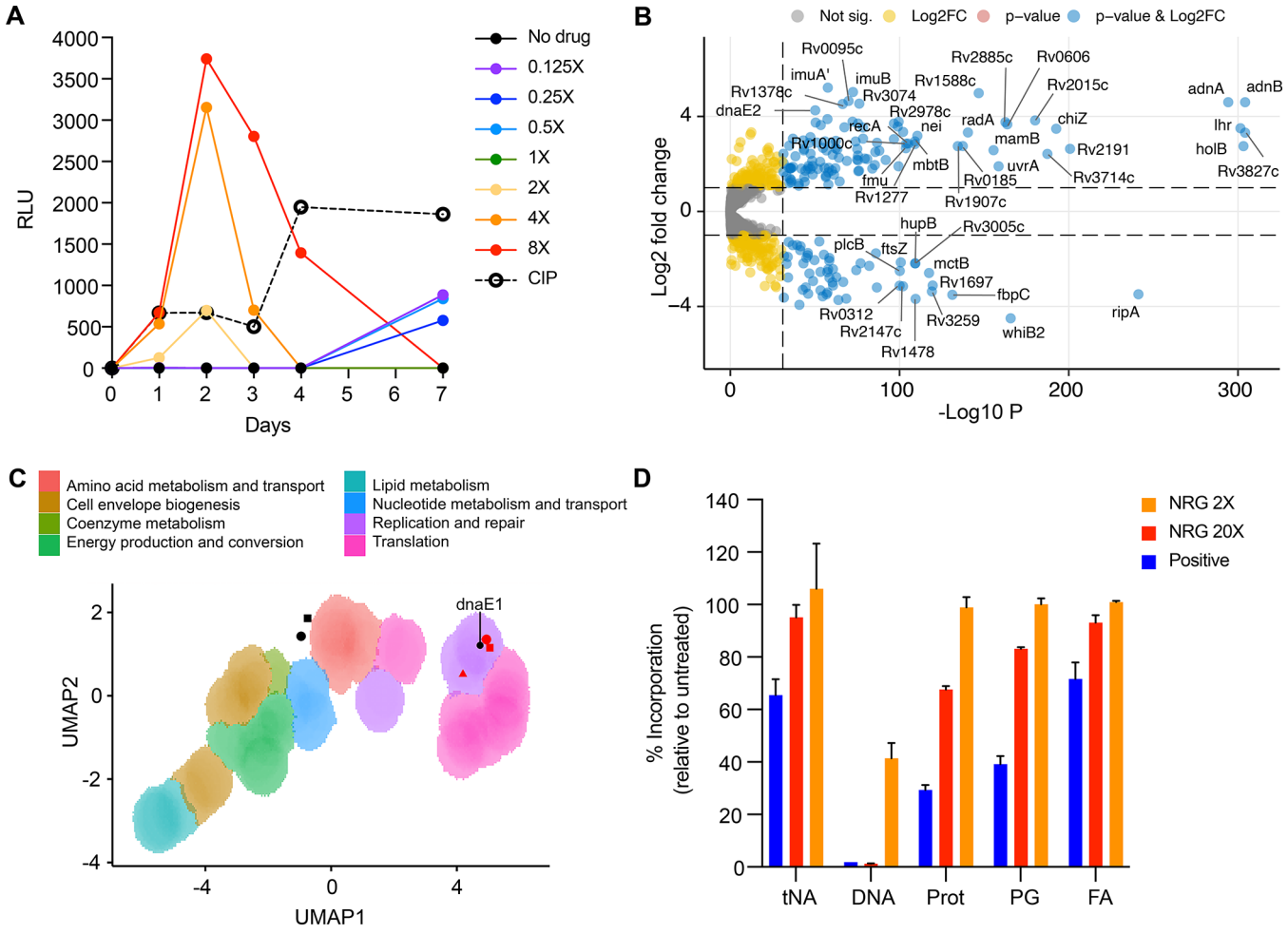

Figure 2. Nargenicin is a genotoxin that inhibits DNA replication in mycobacteria. (A) Analysis of *recA* promoter activity elicited by nargenicin using the reporter strain, PrecA-LUX.[33] Ciprofloxacin (CIP, 2× MIC) was a positive control. RLU, relative luminescence units. (B) Volcano plot illustrating the transcriptional response (RNA-seq) of *Mtb* to nargenicin (10× MIC). Differential expression (Log 2 fold-change) of nargenicin-treated cultures versus dimethyl sulfoxide (DMSO)-treated controls are plotted against adjusted P-values (*P*-value) for each gene, indicating a significant upregulation of genes involved in the response of *Mtb* to DNA-damaging agents.[35] (C) Morphological profiling of *Msm* in response to treatment with nargenicin illustrates that bacillary morphotypes[39] cluster in UMAP space with those of CRISPRi hypomorphs in genes involved in DNA replication, including *dnaE1*. Black circle, untreated; black square, DMSO-treated; red circle, nargenicin-treated at 1× MIC; red square, nargenicin-treated at 2× MIC; and red triangle, nargenicin-treated 4× MIC. (D) Selective inhibition of DNA synthesis by nargenicin in *Mtb*. The incorporation of radiolabeled precursors into the total nucleic acid (tNA), protein (Prot), peptidoglycan (PG), and fatty acid (FA) was measured in the absence (DMSO) or presence of nargenicin at 2× or 20× MIC (black and red bars, respectively). The level of radiolabel incorporation into each macromolecular species is depicted relative to the DMSO-treated control. Assay specificity was confirmed using the following pathway-specific antibiotics as positive controls: ofloxacin (DNA replication; 5 μg/mL), streptomycin (protein synthesis; 10 μg/mL), D-cycloserine (peptidoglycan biosynthesis; 5 μg/mL), and isoniazid (fatty acid biosynthesis; 0.2 μg/mL). Error bars represent the standard deviations from two experimental repeats.

Mycobacterium smegmatis (*Msm*). The activity against *Mtb* diminished significantly when Tween-80 was replaced by Tyloxapol to disperse the mycobacteria. A synergistic effect of Tween-80 has been observed for other TB drugs, most notably rifampicin[26] and streptomycin.[27] The differential potency of nargenicin in media containing Tween-80 *versus* Tyloxapol likely reflects the differential impact of these two detergents on the lipid composition of the cell envelope at the concentrations typically used for clump dispersal[28] with Tween-80 increasing permeability to the drug.[29,30] Nargenicin also showed increased potency in GAST/(Fe)/Tween-80. The *in vitro* selectivity index was reasonable with limited cytotoxicity against the HepG2 cell line (CC50 > 100 μM).

Time−kill kinetic analysis revealed that nargenicin was bactericidal in *Mtb* H37Rv, showing time-dependent kill with limited dose-dependency over the concentration range tested (Figure 1C). To ascertain whether this bactericidal activity was accompanied by cell lysis, we quantified green fluorescent protein (GFP) release from H37Rv-GFP.[31,32] Nargenicin treatment led to GFP release from day 4 onwards, peaking on days 6−7 (Figure 1D). Griselimycin treatment also resulted in delayed GFP release analogous to that elicited by nargenicin, but no release of GFP was observed upon exposure to the DNA gyrase inhibitors, ciprofloxacin, or moxifloxacin, demonstrating that the GFP release was not a generic consequence of disrupting DNA metabolism (Figure 1D).

Nargenicin Inhibits DNA Synthesis and is Genotoxic in *Mtb*. To ascertain whether nargenicin shares the same mechanism of action in mycobacteria as in *S. aureus*,[18] we applied a suite of complementary biological profiling assays in

https://doi.org/10.1021/acsinfecdis.1c00643
ACS Infect. Dis. 2022, 8, 612−625

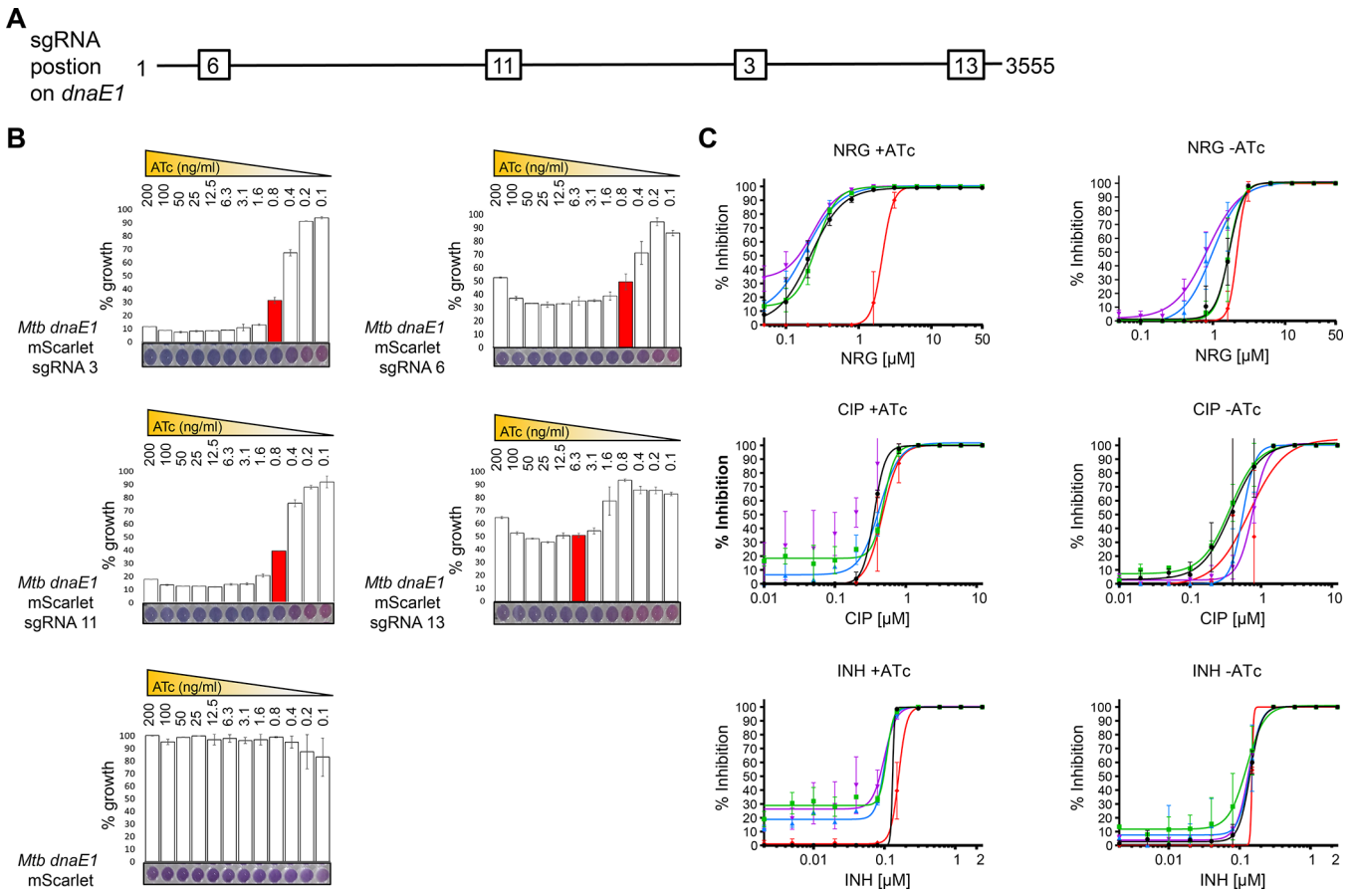

Figure 3. Transcriptional silencing of *dnaE1* by inducible CRISPRi selectively hypersensitizes *Mtb* to nargenicin. (A) Location of sgRNAs 3, 6, 11, and 13 on the *Mtb dnaE1* gene (not drawn to scale). (B) *In vitro* growth phenotypes of the four inducible CRISPRi hypomorphs in *dnaE1* constructed in a strain of *Mtb* carrying a constitutively expressed mScarlet reporter. Strain growth was measured using a microplate alamarBlue assay after 7 days' exposure to ATc at a concentration ranging from 0.1−200 ng/mL. Columns highlighted in red represent the IC_{50} for ATc. Data plotted represent the average and standard deviation of two technical replicates for one of the two independent experiments. (C) The four *dnaE1* hypomorphs were tested for susceptibility to nargenicin (NRG) alongside the control drugs, ciprofloxacin (CIP) and isoniazid (INH). Drug-mediated growth inhibition of the *Mtb dnaE1* mScarlet sgRNA 3 (black), *Mtb dnaE1* mScarlet 6 (green), *Mtb dnaE1* mScarlet sgRNA 11 (blue), *Mtb dnaE1* mScarlet sgRNA 13 (purple) hypomorphs and *Mtb* mScarlet vector control (red) strains in the presence (+ATc, 100 ng/mL) or absence of an inducer (-ATc) was determined by measuring fluorescence intensity at day 14. Data represent the average and standard error of two technical replicates for one representative experiment, fitted with a dose−response curve (nonlinear regression model). Experiments were performed in triplicate.

Mtb and *Msm*. Multiple attempts to isolate spontaneous nargenicin-resistant mutants in *Mtb* or *Msm* by plating 10^9−10^{10} bacilli on media containing nargenicin at 5−20× MIC (*Mtb*) or 1−10× MIC (*Msm*) were unsuccessful, yielding no heritably resistant mutants. Reasoning that nargenicin would elicit a DNA damage response if it disrupts DNA replication, we used the *Mtb* P*recA*-LUX reporter strain to monitor the activity of the DNA-damage-inducible *recA* promoter in response to drug treatment.[33] Like fluoroquinolones and griselimycin, nargenicin triggered dose-dependent induction of luminescence (Figures 2A and S1). Comparative DNA microarray analysis revealed a transcriptomic signature for nargenicin-treated *Mtb* that shared key features with those elicited by mitomycin C and fluoroquinolones (Figures S2A, S2B, and Table S2).[34,35] Genome-wide transcriptome analysis by RNA-seq revealed a profound upregulation of *dnaE2*, *imuA′*, and *imuB*, components of the mycobacterial "mutasome" responsible for DNA damage tolerance and damage-induced mutagenesis[35,36] and other DNA repair and recombination genes, including *recA*, *radA*, *uvrA*, *lhr*, and *adnAB* (Figures 2B, S2C, and Data S1), which are contained in the PafBC regulon.[37] Interestingly, deletion of either *recA*[38] or *dnaE2*[35,36] had a negligible impact on the antimycobacterial activity of nargenicin (Table S1). Genes most highly downregulated by nargenicin were enriched in those associated with cell division (*ftsZ*, *whiB2*, and *ripA*) and included genes involved in cell envelope biogenesis (*e.g.*, *fbpC*) (Figures 2B and S2C).

Morphological profiling of *Msm* exposed to nargenicin revealed a filamentation phenotype with the proportion of elongated bacilli in the population increasing with the drug dose (Figure S3). This drug-induced profile clustered closely in UMAP space with those resulting from transcriptional silencing of components of the DNA replication and repair machinery (Figure 2C), as previously defined,[39] further implicating the disruption of DNA metabolism in the mode of action of nargenicin. Direct evidence for the inhibition of DNA replication was then obtained from a macromolecular incorporation assay, which compares the incorporation of radiolabeled precursors into the total nucleic acid, DNA, protein, peptidoglycan, or fatty acid in cells treated with an experimental drug *versus* controls. Nargenicin had a profound

https://doi.org/10.1021/acsinfecdis.1c00643
ACS Infect. Dis. 2022, 8, 612−625

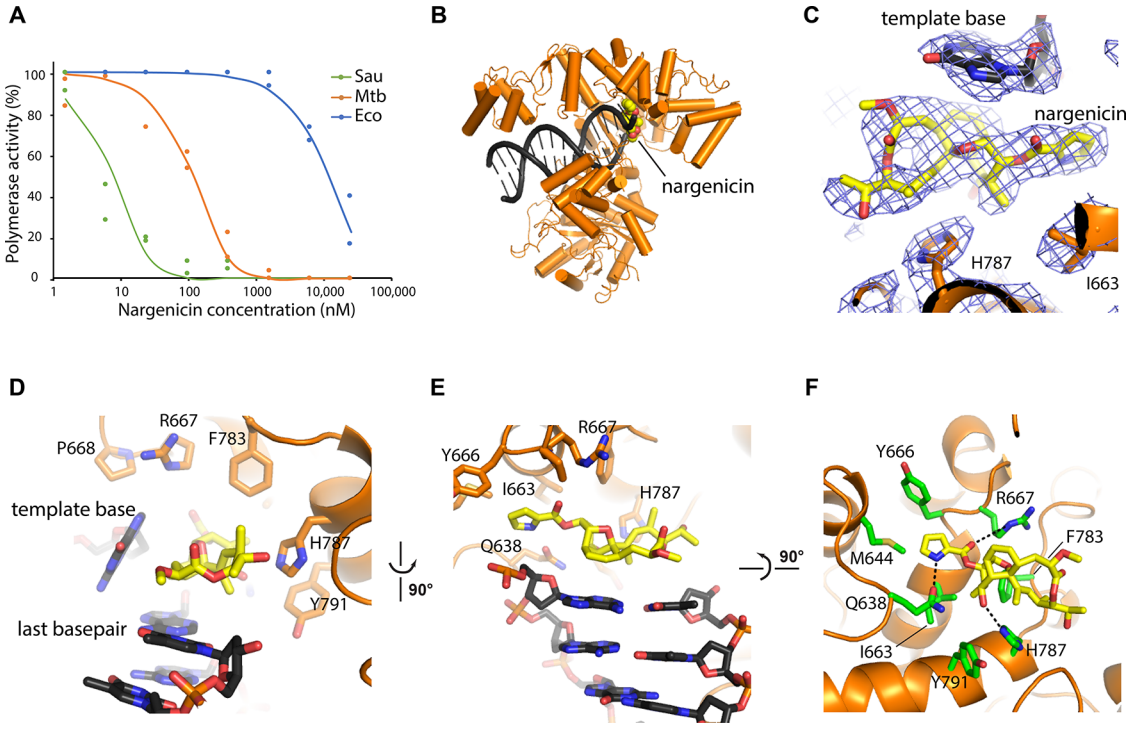

Figure 4. Mechanism of DNA polymerase inhibition by nargenicin. (A) Nargenicin inhibition curves of three bacterial replicative DNA polymerases, *S. aureus* DnaE (green line), *Mtb* DnaE1 (orange line), and *E. coli* Pol IIIα (blue line), show IC_{50} values of 8, 125, and 13 000 nM, respectively. (B) Cryo-EM structure of *Mtb* DnaE1 bound to DNA and nargenicin in yellow. (C) Close-up view of the nargenicin molecule located between the displaced template base and His787. Cryo-EM map is shown in a blue mesh. (D) Composite binding site of nargenicin between the last base pair of the DNA duplex, the displaced templated base, and the fingers domain of the polymerase. (E) Top view of the binding site showing the "base pairing" of nargenicin onto the last base pair of the DNA duplex (ssDNA overhang not shown for clarity). (F) Nargenicin binding pocket in DnaE1 as viewed from the DNA. All residues located with 5 Å of nargenicin are shown in green sticks. Hydrogen bonds between the protein and nargenicin are indicated with black dashed lines.

effect on DNA synthesis resulting in 60% and >95% reduction in [^{3}H]-uracil incorporation when used to treat *Mtb* at 2× and 20× MIC, respectively. In contrast, nargenicin had a limited impact on RNA, protein, peptidoglycan, and fatty acid synthesis (Figure 2D). Together, these results were consistent with the replicative polymerase, DnaE1, as the likely target of nargenicin in mycobacteria.

To investigate this further, we assessed the impact of modulating the level of *dnaE1* expression on the susceptibility of mycobacteria to nargenicin. We generated a set of fluorescently labeled *Mtb* hypomorphs carrying inducible *dnaE1* CRISPR interference (CRISPRi)[40] constructs and determined the inhibitory activity of nargenicin against these strains in the presence or absence of the anhydrotetracycline (ATc) inducer. Marked hypersensitization to nargenicin was observed for all four hypomorphs under conditions of *dnaE1* silencing (+ATc) but not in the uninduced controls (-ATc) (Figure 3A−C). Importantly, the effect was specific to nargenicin, as evidenced by the lack of effect of *dnaE1* silencing on the susceptibility of *Mtb* to isoniazid or ciprofloxacin, which target mycolic acid biosynthesis and DNA gyrase, respectively (Figure 3C). Together, these results identified DnaE1 as a potential target of nargenicin in *Mtb*. Using a vector shown previously to conditionally overexpress *Msm* DnaE1,[41] we found that conditional overexpression of *Msm dnaE1* in *Msm* or *Mtb*, as further confirmed by quantitative real-time polymerase chain reaction (qRT-PCR) analysis (Figure S4C), had no effect on the nargenicin susceptibility of either organism (Figure S4A,B). Therefore, the DnaE1 copy number alone did not determine nargenicin efficacy in mycobacteria.

Nargenicin Differentially Inhibits Bacterial Polymerases. Based on the microbiological evidence, we investigated whether nargenicin inhibited the DNA polymerase activity of *Mtb* DnaE1 in a biochemical assay. For comparison, we included *S. aureus* DnaE, as well as the extensively characterized replicative DNA polymerase from *Escherichia coli*, DNA polymerase III α (Pol IIIα). To monitor the polymerase activity, we used a real-time polymerase assay in which the incorporation of dGMPs in the primer strand quenches the fluorescent signal of a fluorescein group at the 5′ end of the template strand.[41] We found that nargenicin also inhibits the activity of *Mtb* DnaE1, albeit at ∼20-fold higher concentrations than *S. aureus* DnaE (IC_{50} = 125 and 6 nM, respectively) under the conditions of this assay (Figure 4A). Surprisingly, the *E. coli* polymerase was only significantly inhibited by nargenicin at concentrations higher than 10 μM.

Cryo-EM Reveals Mechanism of Inhibition by Nargenicin. To elucidate the mechanism of polymerase inhibition, we determined the structure of full-length *Mtb* DnaE1 in complex with nargenicin and a DNA substrate by cryo-EM (Figures 4B−F and S5). The structure was determined to a resolution of 2.9 Å with well-defined density for the polymerase active site, DNA, and the bound nargenicin molecule (Figure 4B−F). The cryo-EM structure of *Mtb* DnaE1 is identical to the previously determined crystal structure[42] with the exception of the oligonucleotide/oligosaccharide binding (OB) domain that was not included

https://doi.org/10.1021/acsinfecdis.1c00643
ACS Infect. Dis. 2022, 8, 612−625

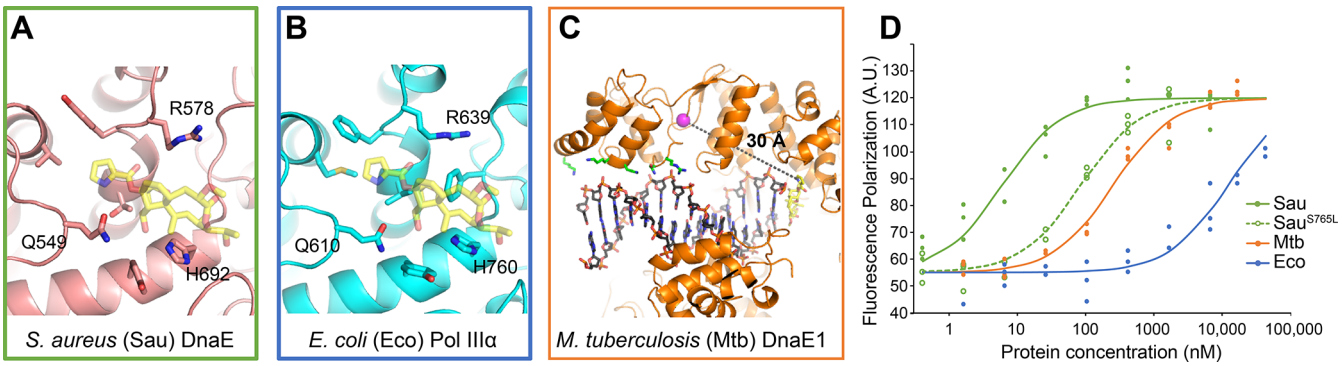

Figure 5. Sensitivity to nargenicin is dependent on the DNA binding affinity. (A) Nargenicin binding site in a computational model of *S. aureus* DnaE. The modeled nargenicin is shown in transparent sticks, and the three residues that make a hydrogen bond to nargenicin in *Mtb* DnaE1 are labeled. The view is identical to Figure 4F. (B) Nargenicin binding site in the crystal structure of *E. coli* Pol III*α*. The modeled nargenicin is shown in transparent sticks, and the three residues that make a hydrogen bond to nargenicin in *Mtb* DnaE1 are labeled. The view is identical to Figure 4F. (C) Nargenicin resistance mutation in *S. aureus* DnaE mapped onto *Mtb* DnaE1, shown by a magenta sphere, is located 30 Å away from the nargenicin (shown in yellow sticks) but is adjacent to the dsDNA binding region of the polymerase. Residues that interact with the DNA backbone are shown in green sticks. (D) Fluorescence anisotropy DNA binding curves of *S. aureus* DnaE (green line), *Mtb* DnaE1 (orange line), and *E. coli* Pol III*α* (blue line) show dissociation constants of 6 nM, 250 nM, and 12 *μ*M, respectively. *S. aureus* DnaE^{S765L} (green dashed line), which carries a mutation that confers antibiotic resistance, shows a dissociation constant of 85 nM, which is ∼14-fold increased, as compared to the wild type.

in the crystal structure (Figure S6). The OB-domain is flexible as it shows a weaker density in the cryo-EM map when compared to the rest of the molecule (Figures S5C and S6C). The flexibility of the OB-domain is consistent with cryo-EM structures of *E. coli* Pol III*α* that show a 70 Å movement of the OB-domain between the DNA-bound and DNA-free state.[43]

The DNA is bound in a canonical manner between the thumb and fingers domains, as was previously observed for other C-family DNA polymerases.[43,44] The nargenicin molecule is bound in the polymerase active site and is sandwiched between the last base pair of the DNA duplex, the first base of the template strand, and the fingers domain of the polymerase (Figure 4D). Nargenicin occupies both the position of the incoming nucleotide as well as the template base and thus mimics the position of the newly synthesized base pair (Figure 4E). To do so, the first unpaired template base is displaced from its position and bumps into Pro668 of an adjacent helix (residues 668 to 673) that becomes disordered. On the protein side, nargenicin occupies a shallow pocket and only makes three direct contacts with the protein: Arg667 and His787 make a hydrogen bond to two oxygens in nargenicin, while Gln638 makes a hydrogen bond with the nitrogen in the pyrrole ring (Figure 4F). The opposite end of nargenicin that is located on top of His787 makes no interaction with the protein as its nearest neighbor is over 5 Å away.

The binding of nargenicin is reminiscent of the binding of aphidicolin in human DNA polymerase *α* (hPol*α*).[45] Although the two inhibitors differ in the structure (Figure S7A) and the polymerases belong to different families (hPol*α* is a B-family polymerase, whereas *Mtb* DnaE1 a C-family polymerase), both inhibitors are bound between the last base pair of the DNA and the polymerase fingers domain, occupy the position of both incoming and templating base, and displace the templating base (Figure S7B,C). However, owing to the structural differences in the polymerase active sites, it is unlikely that nargenicin can inhibit the human polymerase as modeling of nargenicin into the hPol*α* structure reveals several clashes with the protein (Figure S7D). The similar mechanism of action of the two inhibitors is derived from different organisms—aphidicolin is derived from the mold, *Cephalosporium aphidicola*,[45] whereas nargenicin is produced by a *Nocardia* species[19,20]—provides a remarkable example of convergent evolution.

Drug Resistance through Allostery. The structure described above shows that the DNA forms a crucial part of the nargenicin binding site, consistent with the previous observation that binding of nargenicin to *S. aureus* DnaE only occurs in the presence of DNA.[18] This DNA dependency of binding may also hold the key to the differences in inhibition between *S. aureus* DnaE, *Mtb* DnaE1, and *E. coli* Pol III*α* (Figure 5). The predicted nargenicin binding sites for *S. aureus* DnaE and *E. coli* Pol III*α* are highly similar to those of *Mtb* DnaE1 (Figure 5A,B), and the three residues that make a hydrogen bond with nargenicin are conserved in all three species. Hence, the difference in sensitivity does not appear to have its origin in the binding site. Moreover, a mutation in *S. aureus* DnaE (a serine to leucine mutation at position 765, equivalent to *Mtb* DnaE1 residue 860) that renders it resistant to nargenicin is located ∼30 Å away from nargenicin (Figure 5C). This mutation is immediately adjacent to the region of the fingers domain that interacts with the phosphate backbone of the double-stranded DNA substrate. Therefore, we hypothesized that the potency of nargenicin to inhibit a DNA polymerase may be dictated by the polymerase's affinity for DNA. To test this, we measured the DNA affinity of the three polymerases by fluorescence anisotropy using a primed DNA substrate (Figure 5D). The three DNA polymerases show strikingly different dissociation constants of ∼6 nM for *S. aureus* DnaE, 250 nM for *Mtb* DnaE1, and 12 *μ*M for *E. coli* Pol III*α*. Importantly, these DNA affinities correlate with the relative sensitivities to nargenicin, which follow the same trend (Figure 4A). We also tested the resistant mutation in *S. aureus* DnaE (S765L), which, as predicted, reduced the affinity for DNA, approximately 14-fold (Figure 5D).

Taken together, these data support the notion that the potential of nargenicin to inhibit a DNA polymerase is dependent on the polymerase's affinity for DNA, and any changes which reduce the DNA affinity, lead to reduced nargenicin potency, either through natural variation, as in the case of *E. coli* Pol III*α*, or through a resistance-conferring mutation,[18] as for *S. aureus* DnaE. Importantly, *S. aureus*

https://doi.org/10.1021/acsinfecdis.1c00643
ACS Infect. Dis. 2022, 8, 612−625

engages two essential DNA polymerases at the replication fork, namely, PolC and DnaE;[46] if the activity of one is impaired, the other may compensate. However, mycobacteria rely on only one replicative polymerase, DnaE1. Therefore, nargenicin resistance-conferring mutations in DnaE1 could have catastrophic consequences in mycobacteria, which might explain our inability to isolate spontaneous resistant mutants in *Mtb* or *Msm*.

DISCUSSION

We have reported multiple lines of evidence that nargenicin acts as a DNA replication inhibitor in mycobacteria by targeting the essential DnaE1 polymerase, an enzyme identified recently as a highly vulnerable component of the DNA replication machinery in *Mtb*.[9] Unlike the commonly used nucleotide analogues that act as chain terminators through the incorporation into the nascent DNA strand, nargenicin does not become incorporated into the DNA. Instead, it is wedged between the terminal base pair of the DNA substrate and the polymerase fingers domain, occupying both the position of the incoming nucleotide and the templating base, which is displaced by nargenicin. This binding mode is analogous to that of the human Pol α inhibitor, aphidicolin, which is derived from the fungus, *Cephalosporium aphidicola*, and unrelated in structure to nargenicin, indicating that these inhibitors have evolved independently. This unusual mechanism might explain the observation that the antimycobacterial activity of nargenicin was not diminished by overexpression of the cognate target, DnaE1. Based on this mechanism, the DnaE homologue in the *Nocardia* sp. CS682 producer organism would presumably need to bind nargenicin in a DNA-independent manner to fulfill its postulated "decoy" role in self-resistance.[21]

Nargenicin-mediated disruption of replisome function triggers a physiological response in *Mtb*, which resembles that elicited by genotoxins, which cause double-stranded breaks (DSBs) (mitomycin C, fluoroquinolones).[35] This features upregulation of genes encoding the recombinase involved in recombination repair (*recA*), the mutasome responsible for DNA-damage-induced mutagenesis and damage tolerance (*dnaE2*, *imuA′*, *imuB*),[35,36] the PafBC-regulated DSB-resecting motor-nuclease (*adnAB*)[37,47] and a cell wall hydrolase (*chiZ*),[48] among other DNA-damage-responsive genes in mycobacteria. The DNA damage response to nargenicin begs the question of whether pharmacological inhibition of DnaE1 by this or other inhibitors might have the unintended consequence of inducing chromosomal mutations, which could fuel the evolution of drug resistance, as documented for sublethal treatment of mycobacteria and other organisms by fluoroquinolones.[49,50] The concomitant downregulation of *ftsZ*,[39] *sepF*,[51] *whiB2*,[52] and *ripA*[51] is consistent with cellular elongation, resulting from a block in cell division, followed by cell death. Ablation of the SOS response by deletion of *recA*, or a key component thereof (mutasome function) by deletion of *dnaE2*, had no discernible impact on the antimycobacterial activity of nargenicin, suggesting that the LexA/RecA-dependent DNA repair, damage tolerance, and (SOS) mutagenesis systems are unable to rescue mycobacteria from the growth inhibitory effects of nargenicin. Instead, an arrest in cell division, as evidenced by bacillary elongation, appears to precede cell death. However, the DNA damage response to nargenicin also includes genes such as *adnA*, *adnB*, *cho*, and *uvrA*, which form part of the mycobacterial LexA/RecA-independent regulon controlled by PafBC.[37,53] Given that *adnA*, *adnB*, and *lhr* are among the genes most highly upregulated by nargenicin treatment, it will be important to establish whether, under which conditions, and to what extent the functional disruption of this regulon might have on the susceptibility of mycobacteria to this compound.

Another feature of the nargenicin mode of action was the late, strong signal elicited in the GFP release assay. The induction of *chiZ* and downregulation of *fbpC* might be telling in this regard: first, the damage-inducible protein, ChiZ,[54] has been reported to arrest cell division, increase filamentation, and induce cell lysis when overexpressed.[48] Second, inactivation of the mycolyltransferase, FbpC, a member of the antigen 85 complex involved in the synthesis of trehalose dimycolate and mycolylarabinogalactan, which are key components of the mycobacterial cell envelope, has been shown to significantly reduce the mycolate content and increase the permeability of the cell envelope to small hydrophobic and hydrophilic molecules.[55] Thus, in addition to its replication-arresting activity, nargenicin may also compromise the integrity of the mycobacterial outer membrane and thus act as a potentiator of other antitubercular agents whose efficacy is limited by permeation across the mycobacterial cell envelope.

CONCLUSIONS

In conclusion, we have shown that nargenicin mediates its bactericidal activity against *M. tuberculosis* through interaction with DnaE1 in a manner that depends upon the presence of the DNA substrate. In this interaction, the nargenicin molecule wedges itself between DnaE1 and the terminal base pair of the DNA and occupies the place of both the incoming nucleotide and the templating base. By analyzing the physiological consequences of *Mtb* exposure to nargenicin, we show that the arrest in bacillary replication resulting from the nargenicin-DnaE1 interaction triggers induction of a DNA damage response coupled with an arrest in cell division and an apparent weakening of the mycobacterial cell envelope. In addition to strongly reaffirming the value of natural products as a source of novel antitubercular agents, this work has provided the rationale and platform for focusing target-led drug discovery efforts on a promising new TB drug target.

METHODS

Bacterial Strains, Culture Conditions, and Media. The strains used in this study are listed in the **key resources table**. These include the parental wild-type strains, *Mtb* H37Rv[56] and *Msm* mc^{2}155.[57] Clinical isolates were obtained from samples collected from new TB cases and retreatment cases of subjects who were enrolled in a prospective longitudinal cohort study (ClinicalTrials.gov identifier, NCT00341601) at the National Masan Tuberculosis Hospital in the Republic of Korea from May 2005 to December 2006.[58] Mycobacterial strains were cultured in various media depending on the assay. 7H9 OADC was prepared by supplementing Middlebrook 7H9 (Difco) with 10% oleic acid-albumin-dextrose-catalase (OADC) enrichment (Difco), 0.2% glycerol, and either 0.05% Tween-80 (7H9/OADC/Tw) or 0.05% Tyloxapol (7H9/OADC/Tx). 7H9/Glu/ADC/Tw medium was prepared by substituting 10% OADC with 10% albumin-dextrose-catalase (ADC) enrichment (Difco). Similarly, 7H9/Glu/CAS/Tx was prepared by supplementing 7H9 with 0.4% glucose, 0.03%

https://doi.org/10.1021/acsinfecdis.1c00643
ACS Infect. Dis. 2022, 8, 612−625

casitone (CAS), 0.081% NaCl, and 0.05% Tx. Glycerol-alanine-salts with iron (GAST-Fe/Tw) medium, pH 6.6, was prepared with 0.03% CAS, 0.005% ferric ammonium citrate, 0.4% dibasic potassium phosphate, 0.2% citric acid, 0.1% L-alanine, 0.12% $MgCl_2$, 0.06% potassium sulfate, 0.2% ammonium chloride, 0.018% of a 1% sodium hydroxide solution, 1% glycerol, and 0.05% Tween-80. GAST/Tw, an iron limiting media, was prepared as described above but excluding ferric ammonium citrate. All *Mtb* cultures were incubated at 37 °C in sealed culture flasks with no agitation. The cells were plated onto Middlebrook 7H10 agar plates with a 7H10 agar base (Difco) supplemented with 10% OADC and 0.5% glycerol. Unless indicated otherwise, microbiological assays using the strains described below were performed in 7H9/OADC/Tw media.

The fluorescent reporter strain H37Rv-GFP[59] and bioluminescent reporter strain P*recA*-LUX[33] were grown in media supplemented with kanamycin (Kan) at 20 μg/mL, whereas the *Mtb* mScarlet strain and *Msm* ΔL mutant were grown in media supplemented with hygromycin (Hyg) at 50 μg/mL. *Mtb* and *Msm* strains carrying the $P_{UV15\text{-}Tet}$-*dnaE1-MYC*::L5 vector[41] were grown in media containing Kan at 50 μg/mL and supplemented with ATc at 100 ng/mL to induce expression of *dnaE1*. The inducible CRISPRi hypomorphs were grown in media containing Kan (25 μg/mL) and Hyg (50 μg/mL) and supplemented with ATc at 100 ng/mL to induce transcriptional silencing. Minimal inhibitory concentrations (MICs) were determined against a range of clinical isolates: *Mtb* CDC1551;[60] *Mtb* HN878;[61] drug susceptible isolates, *Mtb* 0A029, *Mtb* 0A031 and *Mtb* 0B229; multi-drug resistant isolates, *Mtb* 0B123 resistant to isoniazid (INH^R), ofloxacin (OFX^R), *para*-amino salicylic acid (PAS^R), streptomycin (STR^R), rifampicin (RIF^R); *Mtb* 0A024 (ethambutol (EMB^R), INH^R, kanamycin (KAN^R), PAS^R, pyrazinamide (PZA^R), STR^R, ethionamide (ETH^R), RIF^R, *Mtb* 0B026 (EMB^R, INH^R, KAN^R, PAS^R, RIF^R); and an extensively drug resistant strain, *Mtb* 0B014 (EMB^R, INH^R, KAN^R, OFX^R, PAS^R, RIF^R).[58]

Drug Susceptibility Testing. MIC testing was performed by broth microdilution assay[59] and quantitatively analyzed with the colorimetric alamarBlue cell viability reagent (Thermo Fischer Scientific), as previously described.[32]

Bioluminescence Assay. P*recA*-LUX[33] was grown to an OD_{600} of ∼0.4, diluted 10-fold in 7H9/OADC/Tw, and inoculated into white, clear-bottom, 96-well microtiter plates (Greiner CellStar) containing two-fold serial dilutions of the drug. The plates were incubated at 37 °C, and luminescence was recorded every 24 h for 8 days using a SpectraMax i3x plate reader (Molecular Devices). Data were plotted in Prism 9 (GraphPad).

GFP Release Assay. As described previously,[32] H37Rv-GFP was grown to an OD_{600} of ∼0.3 in 7H9 OADC and exposed to the drug at 1× or 10× MIC. Every 24 h, over a period of 8 days, 200 μL of culture was harvested, pelleted by centrifugation, and the supernatant was transferred to a black, clear-bottom 96-well microtiter plate (Greiner CellStar) and the fluorescence (excitation, 540 nm; emission, 590 nm) was measured using a SpectraMax i3x plate reader (Molecular Devices). Fluorescence intensity was normalized by OD_{650} and standardized to the value of the drug-free control for each sample.

Time−Kill Kinetics. *Mtb* was inoculated in the culture medium at an OD_{600} of 0.002, and the drug was added at a concentration of either 1×, 5×, or 10× MIC. Cultures were incubated in sealed culture flasks, and 1 mL aliquot was harvested every 24 h over 8 days. The samples were washed twice in fresh media. One hundred μL aliquots of 10-fold serial dilutions were plated of 7H11 agar, and colony-forming units (CFUs) were enumerated after incubation for 3−4 weeks.

Macromolecular Incorporation Assays. Macromolecular incorporation assays were performed as described.[62,63] Briefly, *Mtb* cultures were grown to early exponential phase (OD_{600} of ∼0.3) and 1 μCi/mL [^{3}H]-uracil, 2.5 μCi/mL [3H]-phenylalanine, 10 μCi/mL [^{3}H]-N-acetyl glucosamine, and 1 μCi/mL [^{14}C]-acetate were added to quantify the incorporation of the radiolabeled precursors into either total nucleic acid (i.e., DNA and RNA), protein, cell wall, or fatty acids, respectively. The cells were incubated at 37 °C for 1 h, and 150 μL was transferred to 96-well microtiter plates containing 150 μL of each test compound. Nargenicin was used at 2× and 20× MIC with 1% DMSO included as an untreated control. The specificity of assays was monitored by the inclusion of the pathway-specific antibiotics OFX (5 μg/mL), STR (10 μg/mL), D-cycloserine (DCS, 5 μg/mL), and INH (0.2 μg/mL) as positive controls. The assay plates were incubated at 37 °C for 24 h, and precursor incorporation was terminated by the addition of 300 μL of 20% trichloroacetic acid (TCA). The samples were incubated at 4 °C for 1 h, and the precipitates were collected by vacuum filtration with a 96-well MultiScreen GFC glass fiber plate (Millipore). Precipitates were washed three times with 10% TCA, followed by three 95% ethanol washes, and the plates were allowed to air-dry. Precipitates were resuspended in 50 μL of MicroScint 20 (PerkinElmer), and the radioactivity on each filter was measured in a MicroBeta Liquid Scintillation Counter (PerkinElmer). To distinguish between the incorporation of [^{3}H]-uracil into DNA vs. RNA, the RNA was hydrolyzed with 500 μL of 1 M KOH at 37 °C for 16 h and neutralized with 125 μL of HCl. The samples were then precipitated by adding 625 μL of 20% TCA, and the amount of residual radioactivity present in the DNA precipitates was quantified following filtration and washing as described above. All samples were analyzed in duplicate, and the results represent the percentage of radiolabel incorporation relative to the DMSO-treated control from two independent replicates.

Microscopy. *Msm* bacilli were imaged to determine their terminal phenotypes under exposure to varying concentrations of antibiotics as previously described.[39] Strains were grown to late-log phase (OD_{600} of ∼0.8), filtered once through a Millex syringe filter (5 μm pore size, Millipore), and diluted (1:40) into fresh media. The samples were left untreated, exposed to the carrier (DMSO only) or to the varying concentrations of nargenicin in DMSO (1× MIC, 2× MIC, 4× MIC), and incubated for 18 h at 37 °C while shaking. After exposure, the cultures were spotted on low-melt agarose pads and imaged on a ZEISS Axio Observer using a 100×, 1.4 NA objective with Phase Contrast and Colibri 7 fluorescent illumination system. Images were captured using a Zeiss Axiocam 503. Image processing, cell measurements, and analysis were performed in the FIJI Plugin,[64] MicrobeJ,[65] R,[66] and UMAP, as described.[39]

Transcriptional Profiling. Microarray experiments and analyses were performed by the NIAID Microarray Research Facility, as previously described,[35] including two independent samples for each treatment condition. Datasets from cultures exposed to mitomycin C (0.2 μg/mL) and levofloxacin (10 μg/mL) were compared to nargenicin (129 μg/mL). The top

https://doi.org/10.1021/acsinfecdis.1c00643
ACS Infect. Dis. 2022, 8, 612−625

300 upregulated or downregulated genes, ranked by the average Log 2 fold-change in expression data from two biological repeats, were compared to generate gene shortlists common to all three treatments.

For RNA-seq, qRT-PCR, and microarray experiments, *Mtb* cultures (20−30 mL) were grown either in roller bottles or culture flasks on a shaker to mid-exponential phase (OD_{600} of ∼0.3−0.5) prior to treatment with nargenicin at 1× or 10× MIC for 6 h. The cells were harvested by centrifugation at 3000*g* for 10 min and resuspended in 1 mL of Qiazol Lysis Reagent (Qiagen). The cells were lysed with 0.1 mm Zirconia/Silica beads (BioSpec) in a MagNA Lyser Homogenizer (Roche) (6000 rpm, 30 s) three times with 1 min cooling intervals. The samples were centrifuged at 10 000*g* for 5 min at 4 °C, and the supernatant was transferred into a clean tube containing an equal volume of 100% ethanol. The RNA was purified and treated with DNase on-column using the Direct-zol RNA MiniPrep kit (Zymo Research) according to the manufacturer's protocol. The samples were eluted in 50 μL of RNase- and DNase-free water. Purified RNA was treated with DNase for an additional 60 min at 37 °C using the TURBO DNA-free kit (Ambion) according to the manufacturer's protocol. In preparation for microarray analysis and RNA-seq, the sample quality was confirmed using a Bioanalyzer RNA 6000 Nano Kit and Chips (Agilent). For RNA-seq experiments, three independent biological replicates of both nargenicin-treated (10× MIC) and untreated samples were performed. Library preparation and sequencing were done by Admera Health (NJ) using the Illumina NovaSeq S4 sequencing platform. The sequencing strategy included an average of 60 million 150 bp paired-end reads per sample. Reads were demultiplexed to generate raw fastq files for each sample and data were deposited in the NCBI SRA repository (PRJNA722614). Initial quality control (QC) of the raw fastQ files was performed using FastQC.[67] Reads were trimmed and adapters were removed using Trim Galore. Further QC was done by aligning reads using BWA to the reference genome of *Mtb* H37Rv, ASM19595v2, GenBank assembly accession no. GCA_000195955.2 (https://www.ncbi.nlm.nih.gov/assembly/GCF_000195955.2), running RSeQC[68] and dupRadar,[69] and an amalgamated report generated using MultiQC.[70] Transcript quantification was performed using Salmon in a mapping-based mode.[71] Normalization and differential expression analysis were done using DESeq. 2[72] with count normalization by DESeq. 2's median or ratios. *P*-values were adjusted for multiple testing using the Benjamini−Hochberg approach, and genes that displayed an absolute Log 2 fold-change >1 and an adjusted *p*-value <0.05 were considered differentially expressed. Data were visualized in *R*, and the functional enrichment of upregulated and downregulated shortlists as compared to the full genome was performed in STRING[73] using Gene Ontologies, STRING local network clusters, annotated keywords, KEGG pathways, and InterPro protein domains and features as categories. Multiple comparisons were compensated for using the false discovery rate (FDR), with significant enrichment considered as FDR > 0.05.

For qRT-PCR experiments, following TURBO DNase treatment, 250 ng of the RNA was converted to cDNA using SuperScript IV Reverse Transcriptase (Thermo Fischer Scientific). Regions of interest were amplified using primer pairs described in Table S3 and Power SYBR Green PCR master mix (Thermo Fischer Scientific), and transcript levels for three independent samples were quantified on a PikoReal real-time PCR system (Thermo Fischer Scientific). Transcript levels of target genes were normalized to *sigA*.

Construction of Fluorescent dnaE1 Hypomorphs. The ATc-regulated CRISPRi system developed by Rock et al.[40] was used to construct inducible *dnaE1*-targeting *Mtb* hypomorphs carrying the mScarlet fluorescence reporter.[74] Briefly, two oligonucleotides complementary to the dnaE1-targeting sequence (Table S3) were annealed and cloned in pLJR965, and the presence of the sgRNA was confirmed by Sanger sequencing. The sequence-verified constructs were electroporated into *Mtb* mScarlet, selecting on media supplemented with Kan (25 μg/mL) and Hyg (50 μg/mL).

Drug Susceptibility Testing Using Hypomorphs. To assess the impact of *dnaE1* silencing on drug susceptibility, the hypomorphs and vector control strains were grown to an OD_{600} of 1.0 and diluted to an OD_{600} of 0.01 in media either with ATc (200 ng/mL) or without the inducer. Fifty μL of the diluted culture was inoculated into each well of a MIC plate containing 50 μL of media with 2-fold dilutions of the drug. Microtiter plates were incubated at 37 °C for 14 days, and the fluorescence (594 nm, excitation; and 569 nm, emission) was recorded using a Spectramax i3x plate reader. Each strain was normalized to the no-drug control to determine the percentage growth inhibition as a function of drug concentration. Dose−response curves were plotted in Prism 9 (GraphPad).

Protein Expression and Purification. *Mtb* DnaE1 was expressed in *Msm* and purified as previously described.[41] *S. aureus* DnaE and *E. coli* Pol IIIα were expressed in *E. coli* BL21 and purified as previously described.[18,75]

DNA Polymerase Assay. DNA polymerase activity was measured using a real-time polymerase assay as described previously.[41] Briefly, reactions were performed using 5 nM DNA polymerase, 10 nM fluorescently labeled DNA substrate (Primer: 5′-TAGGACGAAGGACTCCCAACTT-TAGGTGCG, Template: 6-FAM-5′-CCCCCCCCCATG-CATGCGCACCTAAAGTTGGGAGTCCTTCGTCCTA), and 100 nM unlabeled DNA substrate (same sequence as above). Reactions contained 100 μM each dNTP, 5 mM $MgSO_4$, 50 mM HEPES pH 7.5, 100 mM potassium glutamate, 2 mM DTT, 0.5 mg/mL BSA, and 10 nM−10 μM nargenicin, diluted from a stock of 10 mM in 100% DMSO. Then, 10 μL reactions were measured for 20 min at 24 °C in a 384-well plate using a Clariostar plate reader (BMG LABTECH) with excitation and emission filters at 485 and 520 nm, respectively.

Fluorescence Anisotropy. DNA binding was measured using a 5 nM Cy3-labeled DNA substrate (Primer: Cy3-5′-GGTAACGCCAGGGTTTTCCCAGTC3, Template 5′-CGCTCACTGGCCGTCGTTTTACAACGTCGT-GACTGGGAAAACCCTGGCGTTACC) and 1 nM−40 μM DNA polymerase. Reaction conditions contained 25 mM HEPES (pH 7.5), 50 mM potassium glutamate, 2 mM DTT, and 0.5 mg/mL BSA. Then, 10 μL reactions were measured at 24 °C in a 384-well plate using a Clariostar plate reader with excitation and emission filters at 540 and 590 nm, respectively.

Cryo-EM Sample Preparation and Imaging. Purified *Mtb* DnaE1 was diluted to 4 μM in 20 mM PIPES (pH 7.0), 50 mM potassium glutamate, 5 mM $MgCl_2$, 2 mM DTT, and 0.01% Tween-20. The diluted protein was incubated for 5 min with 10 μM nargenicin (diluted from a stock of 10 mM in 100% DMSO) and 20 μM DNA substrate (Template: 5′-GATAGAGCAGAAGGACGAAGGACTCCCAACTT-

https://doi.org/10.1021/acsinfecdis.1c00643
ACS Infect. Dis. 2022, 8, 612−625

TAGGTG, Primer: 5′-GCACCTAAAGTTGG-GAGTCCTTCGTCCT*T, where the asterisk marks the position of a phosphorothioate bond). Then, 3 μL of sample were adsorbed onto glow-discharged copper R2/1 holey carbon grids (Quantifoil). Grids were glow discharged for 45 s at 25 mA using an EMITECH K950 apparatus. Grids were blotted for one second at ∼80% humidity at 4 °C and flash-frozen in liquid ethane using a Leica EM GP plunge freezer. The grids were loaded into a Titan Krios (FEI) electron microscope operating at 300 kV with a Gatan K3 detector. The slit width of the energy filter was set to 20 eV. Images were recorded with EPU software (Thermo Fisher Scientific) in the counting mode. Dose, magnification, and pixel size are detailed in Table 1.

Table 1. Cryo-EM Data Collection, Refinement, and Validation Statistics

data collection and processing		model comparison	
magnification	×105 000	nonhydrogen atoms	8990
voltage (kV)	300	protein residues	1070
electron exposure $e^-/Å^2$	54	B factors (Å^2)	
defocus range (μm)	0.8−2.0	protein	21−306
pixel size (Å)	0.859	r.m.s deviations	
symmetry imposed	C1	bond lengths (Å^2)	0.0126
initial particle images (no)	2000000	bond angles (°)	1.1569
final particle images (no)	196709	validation	
map resolution (Å)	2.8	MolProbity score	1.47
FSC threshold	0.143	clashscore	4.22
map resolution range (Å)	2.8 to > 5.5	poor rotamers (%)	1.28
refinement		Ramachandran plot	
initial model used	5LEW	favored (%)	96.90
model resolution (Å)	2.9	allowed (%)	3.10
FSC threshold	0.143	disallowed (%)	0
map sharpening B-factor (Å^2)	−50		

Cryo-EM Image Processing. All image processing was performed using RELION 3.1.[76] The images were drift corrected using RELION's own (CPU-based) implementation of the UCSF motioncor2, and defocus was estimated using gCTF.[77] LoG-based auto-picking was performed on all micrographs, and picked particles were 2D classified. After three rounds of 2D classification, classes with different orientations were selected for initial model generation in RELION. The initial model was used as a reference for 3D classification into different classes. The selected classes from 3D classification were subjected to 3D auto refinement followed by different rounds of CTF refinement plus a final round of Bayesian polishing. Polished particles were used for the 3D auto-refine job, and the final map was postprocessed to correct for the modulation transfer function of the detector and sharpened by applying a negative B-factor manually set to −50. A soft mask was applied during postprocessing to generate FSC curves to produce a map of an average resolution of 2.9 Å. The RELION postprocessed map was used to generate improved-resolution EM maps using the SuperEM method,[78] which aided in model building and refinement. Model building was performed using Coot,[79] REFMAC5,[80] the CCPEM-suite,[81] and Phenix.[82] Details on model refinement and validation are shown in Table 1. In brief, model building started by the rigid-body fitting of the known DnaE1 crystal structure (PDB 5LEW)[42] into the experimental density map using Coot. The DNA molecule was generated, and the rigid body was fitted into the experimental density map using Coot. Next, we carried out one round of refinement in REFMAC5 using jelly-body restraints, and the model was further manually adjusted in Coot. Final refinement and model validation were performed using Phenix.

Quantification and Statistical Analysis. Statistical details are given in the Methods sections and figure legends, and these include details of the experiments, numbers of replicates (technical and/or experimental), statistical software used, and thresholds of significance. Significance was generally determined as $p<0.05$, and correction for multiple comparisons was performed, as appropriate. Independent experiments were performed a minimum of two times, and these data were utilized for the generation of summary statistics (mean and standard deviation). Replicate data are included within each figure, as indicated in figure legends, else data are described as a representative experiment. In addition, DNA polymerase assays and DNA binding experiments were performed in three or more independent experiments. Data were not excluded from experimental datasets prior to or during analyses other than during cryo-EM data processing, where particles that did not possess high-resolution features were removed following standard procedures for cryo-EM structure determination.

■ ASSOCIATED CONTENT

Supporting Information

The Supporting Information is available free of charge at https://pubs.acs.org/doi/10.1021/acsinfecdis.1c00643.

Comparison of the transcriptional response of *Mtb* to nargenicin *versus* other genotoxins; binding of aphidicolin in human Pol α; antimycobacterial activity of nargenicin; primers and other oligonucleotides (figures and tables) (PDF)

Dataset S1 comprises output gene lists of RNA-seq differential gene expression analysis and STRING functional analysis of significantly differentially expressed genes (Data S1); related to Figure 2 and C (XLSX)

Accession Codes

NCBI Sequence Read Archive (SRA) repository (PRJNA722614).

■ AUTHOR INFORMATION

Corresponding Authors

Meindert H. Lamers − *Cell and Chemical Biology, Leiden University Medical Center, 2333 ZC Leiden, The Netherlands*; Email: m.h.lamers@lumc.nl

Valerie Mizrahi − *SAMRC/NHLS/UCT Molecular Mycobacteriology Research Unit, DST/NRF Centre of Excellence for Biomedical TB Research, Institute of Infectious Disease and Molecular Medicine and Department of Pathology, Faculty of Health Sciences, University of Cape Town, Observatory 7925, South Africa*; orcid.org/0000-0003-4824-9115; Email: valerie.mizrahi@uct.ac.za

Authors

Melissa D. Chengalroyen − *SAMRC/NHLS/UCT Molecular Mycobacteriology Research Unit, DST/NRF Centre of Excellence for Biomedical TB Research, Institute of Infectious Disease and Molecular Medicine and Department of Pathology, Faculty of Health Sciences, University of Cape Town, Observatory 7925, South Africa*

https://doi.org/10.1021/acsinfecdis.1c00643
ACS Infect. Dis. 2022, 8, 612−625

Mandy K. Mason − *SAMRC/NHLS/UCT Molecular Mycobacteriology Research Unit, DST/NRF Centre of Excellence for Biomedical TB Research, Institute of Infectious Disease and Molecular Medicine and Department of Pathology, Faculty of Health Sciences, University of Cape Town, Observatory 7925, South Africa*

Alessandro Borsellini − *Cell and Chemical Biology, Leiden University Medical Center, 2333 ZC Leiden, The Netherlands*

Raffaella Tassoni − *Cell and Chemical Biology, Leiden University Medical Center, 2333 ZC Leiden, The Netherlands*

Garth L. Abrahams − *SAMRC/NHLS/UCT Molecular Mycobacteriology Research Unit, DST/NRF Centre of Excellence for Biomedical TB Research, Institute of Infectious Disease and Molecular Medicine and Department of Pathology, Faculty of Health Sciences, University of Cape Town, Observatory 7925, South Africa; Tuberculosis Research Section, Laboratory of Clinical Immunology and Microbiology, National Institute of Allergy and Infectious Disease, National Institutes of Health, Bethesda, Maryland 20892, United States;* Present Address: Department of Biochemistry and Microbiology, Rhodes University, Grahamstown 6139, South Africa

Sasha Lynch − *SAMRC/NHLS/UCT Molecular Mycobacteriology Research Unit, DST/NRF Centre of Excellence for Biomedical TB Research, Institute of Infectious Disease and Molecular Medicine and Department of Pathology, Faculty of Health Sciences, University of Cape Town, Observatory 7925, South Africa*

Yong-Mo Ahn − *Tuberculosis Research Section, Laboratory of Clinical Immunology and Microbiology, National Institute of Allergy and Infectious Disease, National Institutes of Health, Bethesda, Maryland 20892, United States*

Jon Ambler − *Wellcome Centre for Infectious Diseases Research in Africa, University of Cape Town, Observatory 7925, South Africa*

Katherine Young − *Infectious Disease, Merck & Co. Inc., West Point, Pennsylvania 19446, United States*

Brendan M. Crowley − *Discovery Chemistry, Merck & Co. Inc., West Point, Pennsylvania 19446, United States*

David B. Olsen − *Infectious Disease, Merck & Co. Inc., West Point, Pennsylvania 19446, United States*

Digby F. Warner − *SAMRC/NHLS/UCT Molecular Mycobacteriology Research Unit, DST/NRF Centre of Excellence for Biomedical TB Research, Institute of Infectious Disease and Molecular Medicine and Department of Pathology, Faculty of Health Sciences, University of Cape Town, Observatory 7925, South Africa;* orcid.org/0000-0002-4146-0930

Clifton E. Barry III − *Tuberculosis Research Section, Laboratory of Clinical Immunology and Microbiology, National Institute of Allergy and Infectious Disease, National Institutes of Health, Bethesda, Maryland 20892, United States*

Helena I. M. Boshoff − *Tuberculosis Research Section, Laboratory of Clinical Immunology and Microbiology, National Institute of Allergy and Infectious Disease, National Institutes of Health, Bethesda, Maryland 20892, United States;* orcid.org/0000-0002-4333-206X

Complete contact information is available at: https://pubs.acs.org/10.1021/acsinfecdis.1c00643

Author Contributions

[▽]M.D.C. and M.K.M. contributed equally to this paper. M.D.C. and M.K.M. performed the microbiological profiling and RNA-seq experiments and analyses; G.L.A. and H.I.M.B. performed the DNA microarray and macromolecular incorporation assays; R.T. performed the polymerase assays; A.B. and M.H.L. performed the cryo-EM; J.A. provided bioinformatics support; and S.L. and Y.-M.A. provided technical support. The experiments were designed and the data were analyzed by M.D.C., M.K.M., G.L.A., B.M.C., D.B.O., D.F.W., C.E.B.III, H.I.M.B., M.H.L., and V.M. This manuscript was written by M.D.C., M.K.M., M.H.L., and V.M., and all authors read and edited it. M.H.L., D.B.O., C.E.B.III, and V.M. were Team Leads.

Notes

The authors declare the following competing financial interest(s): B.M.C, K.Y. and D.B.O. are employees of Merck Sharp & Dohme Corp., a subsidiary of Merck & Co., Inc., Kenilworth, NJ, USA. C.E.B.III and V.M. are members of the Editorial Advisory Board of *ACS Infectious Diseases*.

Plasmids and bacterial strains generated for this study are available upon request.

RNA-seq datasets from this study are deposited in the NCBI Sequence Read Archive (SRA) repository (PRJNA722614) and are publicly available as of the date of publication. Atomic models and cryo-EM maps have been deposited to the Protein Data Bank and the Electron Microscopy Database under accession codes PDB 7PU7 and EMD 13654. The paper does not report the original code. The pipeline for RNA-seq analysis can be found at the GitHub repository (https://github.com/jambler24/bacterial_transcriptomics). Microscopy data are available from the lead contact upon request. Any additional information required to reanalyze the data reported in this paper is available from the lead contact upon request.

■ ACKNOWLEDGMENTS

This work was supported by grants from the Bill & Melinda Gates Foundation (OPP1158806 to C.E.B.III and V.M.; INV-004757 to V.M. and INV-002474 to M.H.L.), the Broad Institute (Turning the Tide Against Tuberculosis program), the South African Medical Research Council, the National Research Foundation of South Africa, the Oppenheimer Memorial Trust, and an International Research Scholar's grant from the HHMI (#55007649) (to V.M.), an African Career Accelerator Award from the Crick African Network (to M.K.M.), and, in part, by the Intramural Research Program of NIAID (to H.I.M.B. and C.E.B.III). We acknowledge the use of the ilifu cloud computing facility (www.ilifu.ac.za) and thank Timothy de Wet for advice and assistance with morphotyping experimentation and analysis, Dirk Schnappinger and Jeremy Rock for kindly providing reagents, and Curtis Englehart for technical advice.

■ ABBREVIATIONS USED

ATc, anhydrotetracycline; cryo-EM, cryo-electron microscopy; DSB, double-stranded breaks; GFP, green fluorescent protein; MDR, multidrug resistant; MIC, minimum inhibitory concentration; *Msm*, *Mycobacterium smegmatis*; *Mtb*, *Mycobacterium tuberculosis*; OB, oligonucleotide/oligosaccharide binding; Pol IIIα, DNA polymerase III α; TB, tuberculosis; TBDA, Tuberculosis Drug Accelerator

REFERENCES

(1) WHO. *Global Tuberculosis Report 2021*; World Health Organisation, 2021.

(2) Conradie, F.; Diacon, A. H.; Ngubane, N.; Howell, P.; Everitt, D.; Crook, A. M.; Mendel, C. M.; Egizi, E.; Moreira, J.; Timm, J.; McHugh, T. D.; Wills, G. H.; Bateson, A.; Hunt, R.; Van Niekerk, C.; Li, M.; Olugbosi, M.; Spigelman, M. Treatment of highly drug-resistant pulmonary tuberculosis. *N. Engl. J. Med.* **2020**, *382*, 893−902.

(3) Dorman, S. E.; Nahid, P.; Kurbatova, E. V.; Phillips, P. P. J.; Bryant, K.; Dooley, K. E.; Engle, M.; Goldberg, S. V.; Phan, H. T. T.; Hakim, J.; Johnson, J. L.; Lourens, M.; Martinson, N. A.; Muzanyi, G.; Narunsky, K.; Nerette, S.; Nguyen, N. V.; Pham, T. H.; Pierre, S.; Purfield, A. E.; Samaneka, W.; Savic, R. M.; Sanne, I.; Scott, N. A.; Shenje, J.; Sizemore, E.; Vernon, A.; Waja, Z.; Weiner, M.; Swindells, S.; Chaisson, R. E. Four-month rifapentine regimens with or without moxifloxacin for tuberculosis. *N. Engl. J. Med.* **2021**, *384*, 1705−1718.

(4) Evans, J. C.; Mizrahi, V. Priming the tuberculosis drug pipeline: new antimycobacterial targets and agents. *Curr. Opin. Microbiol.* **2018**, *45*, 39−46.

(5) Aldridge, B. B.; Barros-Aguirre, D.; Barry, C. E.; Bates, R. H.; Berthel, S. J.; Boshoff, H. I.; Chibale, K.; Chu, X.-J.; Cooper, C. B.; Dartois, V.; Duncan, K.; Fotouhi, N.; Gusovsky, F.; Hipskind, P. A.; Kempf, D. J.; Lelièvre, J.; Lenaerts, A. J.; McNamara, C. W.; Mizrahi, V.; Nathan, C.; Olsen, D. B.; Parish, T.; Petrassi, H. M.; Pym, A.; Rhee, K. Y.; Robertson, G. T.; Rock, J. M.; Rubin, E. J.; Russell, B.; Russell, D. G.; Sacchettini, J. C.; Schnappinger, D.; Schrimpf, M.; Upton, A. M.; Warner, P.; Wyatt, P. G.; Yuan, Y. The Tuberculosis Drug Accelerator at year 10: what have we learned? *Nat. Med.* **2021**, *27*, 1333−1337.

(6) Reiche, M. A.; Warner, D. F.; Mizrahi, V. Targeting DNA replication and repair for the development of novel therapeutics against tuberculosis. *Front. Mol. Biosci.* **2017**, *4*, 75.

(7) Ditse, Z.; Lamers, M. H.; Warner, D. F. DNA replication in *Mycobacterium tuberculosis*. *Microbiol. Spectrum* **2017**, *5* (2), 1−25.

(8) de Wet, T. J.; Warner, D. F.; Mizrahi, V. Harnessing biological insight to accelerate tuberculosis drug discovery. *Acc. Chem. Res.* **2019**, *52*, 2340−2348.

(9) Bosch, B.; DeJesus, M. A.; Poulton, N. C.; Zhang, W.; Engelhart, C. A.; Zaveri, A.; Lavalette, S.; Ruecker, N.; Trujillo, C.; Wallach, J. B.; Li, S.; Ehrt, S.; Chait, B. T.; Schnappinger, D.; Rock, J. M. Genome-wide gene expression tuning reveals diverse vulnerabilities of *M. tuberculosis*. *Cell* **2021**, *184*, 4579−4592 e4524.

(10) Mayer, C.; Takiff, H. The molecular genetics of fluoroquinolone resistance in *Mycobacterium tuberculosis*. In *Molecular Genetics of Mycobacteria*; John Wiley & Sons, Inc., 2014; pp 455−478.

(11) Nagaraja, V.; Godbole, A. A.; Henderson, S. R.; Maxwell, A. DNA topoisomerase I and DNA gyrase as targets for TB therapy. *Drug Discovery Today* **2017**, *22*, 510−518.

(12) Dawson, R.; Diacon, A. H.; Everitt, D.; van Niekerk, C.; Donald, P. R.; Burger, D. A.; Schall, R.; Spigelman, M.; Conradie, A.; Eisenach, K.; Venter, A.; Ive, P.; Page-Shipp, L.; Variava, E.; Reither, K.; Ntinginya, N. E.; Pym, A.; von Groote-Bidlingmaier, F.; Mendel, C. M. Efficiency and safety of the combination of moxifloxacin, pretomanid (PA-824), and pyrazinamide during the first 8 weeks of antituberculosis treatment: a phase 2b, open-label, partly randomised trial in patients with drug-susceptible or drug-resistant pulmonary tuberculosis. *Lancet* **2015**, *385*, 1738−1747.

(13) Das, S.; Garg, T.; Srinivas, N.; Dasgupta, A.; Chopra, S. Targeting DNA gyrase to combat *Mycobacterium tuberculosis*: An update. *Curr. Top. Med. Chem.* **2019**, *19*, 579−593.

(14) Johnson, E. O.; LaVerriere, E.; Office, E.; Stanley, M.; Meyer, E.; Kawate, T.; Gomez, J. E.; Audette, R. E.; Bandyopadhyay, N.; Betancourt, N.; Delano, K.; Da Silva, I.; Davis, J.; Gallo, C.; Gardner, M.; Golas, A. J.; Guinn, K. M.; Kennedy, S.; Korn, R.; McConnell, J. A.; Moss, C. E.; Murphy, K. C.; Nietupski, R. M.; Papavinasasundaram, K. G.; Pinkham, J. T.; Pino, P. A.; Proulx, M. K.; Ruecker, N.; Song, N.; Thompson, M.; Trujillo, C.; Wakabayashi, S.; Wallach, J. B.; Watson, C.; Ioerger, T. R.; Lander, E. S.; Hubbard, B. K.; Serrano-Wu, M. H.; Ehrt, S.; Fitzgerald, M.; Rubin, E. J.; Sassetti, C. M.; Schnappinger, D.; Hung, D. T. Large-scale chemical-genetics yields new *M. tuberculosis* inhibitor classes. *Nature* **2019**, *571*, 72−78.

(15) Godbole, A. A.; Ahmed, W.; Bhat, R. S.; Bradley, E. K.; Ekins, S.; Nagaraja, V. Targeting *Mycobacterium tuberculosis* topoisomerase I by small-molecule inhibitors. *Antimicrob. Agents Chemother.* **2015**, *59*, 1549−1557.

(16) Kaguni, J. M. The macromolecular machines that duplicate the *Escherichia coli* chromosome as targets for drug discovery. *Antibiotics* **2018**, *7*, 23.

(17) Kling, A.; Lukat, P.; Almeida, D. V.; Bauer, A.; Fontaine, E.; Sordello, S.; Zaburannyi, N.; Herrmann, J.; Wenzel, S. C.; König, C.; Ammerman, N. C.; Barrio, M. B.; Borchers, K.; Bordon-Pallier, F.; Brönstrup, M.; Courtemanche, G.; Gerlitz, M.; Geslin, M.; Hammann, P.; Heinz, D. W.; Hoffmann, H.; Klieber, S.; Kohlmann, M.; Kurz, M.; Lair, C.; Matter, H.; Nuermberger, E.; Tyagi, S.; Fraisse, L.; Grosset, J. H.; Lagrange, S.; Müller, R. Targeting DnaN for tuberculosis therapy using novel griselimycins. *Science* **2015**, *348*, 1106−1112.

(18) Painter, R. E.; Adam, G. C.; Arocho, M.; DiNunzio, E.; Donald, R. G. K.; Dorso, K.; Genilloud, O.; Gill, C.; Goetz, M.; Hairston, N. N.; Murgolo, N.; Nare, B.; Olsen, D. B.; Powles, M.; Racine, F.; Su, J.; Vicente, F.; Wisniewski, D.; Xiao, L.; Hammond, M.; Young, K. Elucidation of dnaE as the antibacterial target of the natural product, nargenicin. *Chem. Biol.* **2015**, *22*, 1362−1373.

(19) Cane, D. E.; Yang, C. C. Nargenicin biosynthesis: late stage oxidations and absolute configuration. *J. Antibiot.* **1985**, *38*, 423−426.

(20) Celmer, W. D.; Chmurny, G. N.; Moppett, C. E.; Ware, R. S.; Watts, P. C.; Whipple, E. B. Structure of natural antibiotic CP-47,444. *J. Am. Chem. Soc.* **1980**, *102*, 4203−4209.

(21) Pidot, S. J.; Rizzacasa, M. A. The nargenicin family of oxa-bridged macrolide antibiotics. *Chem. − Eur. J.* **2020**, *26*, 2780−2792.

(22) Sohng, J. K.; Yamaguchi, T.; Seong, C. N.; Baik, K. S.; Park, S. C.; Lee, H. J.; Jang, S. Y.; Simkhada, J. R.; Yoo, J. C. Production, isolation and biological activity of nargenicin from Nocardia sp. CS682. *Arch. Pharmacal Res.* **2008**, *31*, 1339−1345.

(23) Dhakal, D.; Han, J. M.; Mishra, R.; Pandey, R. P.; Kim, T. S.; Rayamajhi, V.; Jung, H. J.; Yamaguchi, T.; Sohng, J. K. Characterization of tailoring steps of nargenicin A1 biosynthesis reveals a novel analogue with anticancer activities. *ACS Chem. Biol.* **2020**, *15*, 1370−1380.

(24) Dhakal, D.; Rayamajhi, V.; Nguyen, H. T.; Poudel, P. B.; Sohng, J. K. Complete genome sequence of Nocardia sp. strain CS682, a producer of antibacterial compound nargenicin A1. *Microbiol. Resour. Announce.* **2019**, *8*, No. e01098.

(25) Young, K.; Olsen, D. B.; Singh, S. B.; Su, J.; Wilkening, R. R.; Apgar, J. M.; Meng, D.; Parker, D.; Mandal, M.; Yang, L.; Painter, R. E.; Dang, Q.; Suzuki, T. Nargenicin compounds and uses thereof as antibacterial agents. United States US20170305924A1, 2017.

(26) Lorian, V.; Finland, M. In vitro effect of rifampin on Mycobacteria. *Appl. Microbiol.* **1969**, *17*, 202−207.

(27) Yamori, S.; Tsukamura, M. Paradoxical effect of tween 80 between the susceptibility to rifampicin and streptomycin and the susceptibility to ethambutol and sulfadimethoxine in the Mycobacterium avium-Mycobacterium intracellulare Complex. *Microbiol. Immunol.* **1991**, *35*, 921−926.

(28) Ortalo-Magné, A.; Lemassu, A.; Laneelle, M. A.; Bardou, F.; Silve, G.; Gounon, P.; Marchal, G.; Daffe, M. Identification of the surface-exposed lipids on the cell envelopes of *Mycobacterium tuberculosis* and other mycobacterial species. *J. Bacteriol.* **1996**, *178*, 456−461.

(29) Piddock, L. J.; Williams, K. J.; Ricci, V. Accumulation of rifampicin by *Mycobacterium aurum*, *Mycobacterium smegmatis* and *Mycobacterium tuberculosis*. *J. Antimicrob. Chemother.* **2000**, *45*, 159−165.

(30) Tullius, M. V.; Nava, S.; Horwitz, M. A. PPE37 Is essential for *Mycobacterium tuberculosis* heme-iron acquisition (HIA), and a defective PPE37 in *Mycobacterium bovis* BCG prevents HIA. *Infect. Immun.* **2019**, *87*, No. e00540.

https://doi.org/10.1021/acsinfecdis.1c00643
ACS Infect. Dis. 2022, 8, 612−625

(31) Kumar, P.; Arora, K.; Lloyd, J. R.; Lee, I. Y.; Nair, V.; Fischer, E.; Boshoff, H. I.; Barry, C. E., 3rd Meropenem inhibits D,D-carboxypeptidase activity in *Mycobacterium tuberculosis*. *Mol. Microbiol.* **2012**, *86*, 367−381.
(32) Chengalroyen, M. D.; Jordaan, A.; Seldon, R.; Ioerger, T.; Franzblau, S. G.; Nasr, M.; Warner, D. F.; Mizrahi, V. Biological profiling enables rapid mechanistic classification of phenotypic screening hits and identification of KatG activation-dependent pyridine carboxamide prodrugs with activity against *Mycobacterium tuberculosis*. *Front Cell. Infect. Microbiol.* **2020**, *10*, No. 582416.
(33) Naran, K.; Moosa, A.; Barry, C. E.; Boshoff, H. I. M.; Mizrahi, V.; Warner, D. F. Bioluminescent reporters for rapid mechanism of action assessment in tuberculosis drug discovery. *Antimicrob. Agents Chemother.* **2016**, *60*, 6748−6757.
(34) Boshoff, H. I.; Myers, T. G.; Copp, B. R.; McNeil, M. R.; Wilson, M. A.; Barry, C. E., 3rd The transcriptional responses of *Mycobacterium tuberculosis* to inhibitors of metabolism: novel insights into drug mechanisms of action. *J. Biol. Chem.* **2004**, *279*, 40174−40184.
(35) Boshoff, H. I.; Reed, M. B.; Barry, C. E., 3rd; Mizrahi, V. DnaE2 polymerase contributes to in vivo survival and the emergence of drug resistance in *Mycobacterium tuberculosis*. *Cell* **2003**, *113*, 183−193.
(36) Warner, D. F.; Ndwandwe, D. E.; Abrahams, G. L.; Kana, B. D.; Machowski, E. E.; Venclovas, C.; Mizrahi, V. Essential roles for imuA'- and imuB-encoded accessory factors in DnaE2-dependent mutagenesis in *Mycobacterium tuberculosis*. *Proc. Natl. Acad. Sci. U.S.A.* **2010**, *107*, 13093−13098.
(37) Müller, A. U.; Imkamp, F.; Weber-Ban, E. The Mycobacterial LexA/RecA-independent DNA damage response Is controlled by PafBC and the pup-proteasome system. *Cell Rep.* **2018**, *23*, 3551−3564.
(38) Machowski, E. E.; Barichievy, S.; Springer, B.; Durbach, S. I.; Mizrahi, V. In vitro analysis of rates and spectra of mutations in a polymorphic region of the Rv0746 PE_PGRS gene of *Mycobacterium tuberculosis*. *J. Bacteriol.* **2007**, *189*, 2190−2195.
(39) de Wet, T. J.; Winkler, K. R.; Mhlanga, M.; Mizrahi, V.; Warner, D. F. Arrayed CRISPRi and quantitative imaging describe the morphotypic landscape of essential mycobacterial genes. *eLife* **2020**, *9*, No. e60083.
(40) Rock, J. M.; Hopkins, F. F.; Chavez, A.; Diallo, M.; Chase, M. R.; Gerrick, E. R.; Pritchard, J. R.; Church, G. M.; Rubin, E. J.; Sassetti, C. M.; Schnappinger, D.; Fortune, S. M. Programmable transcriptional repression in mycobacteria using an orthogonal CRISPR interference platform. *Nat. Microbiol.* **2017**, *2*, No. 16274.
(41) Rock, J. M.; Lang, U. F.; Chase, M. R.; Ford, C. B.; Gerrick, E. R.; Gawande, R.; Coscolla, M.; Gagneux, S.; Fortune, S. M.; Lamers, M. H. DNA replication fidelity in *Mycobacterium tuberculosis* is mediated by an ancestral prokaryotic proofreader. *Nat. Genet.* **2015**, *47*, 677−681.
(42) Baños-Mateos, S.; van Roon, A.-M. M.; Lang, U. F.; Maslen, S. L.; Skehel, J. M.; Lamers, M. H. High-fidelity DNA replication in *Mycobacterium tuberculosis* relies on a trinuclear zinc center. *Nat. Commun.* **2017**, *8*, No. 855.
(43) Fernandez-Leiro, R.; Conrad, J.; Scheres, S. H.; Lamers, M. H. cryo-EM structures of the E. coli replicative DNA polymerase reveal its dynamic interactions with the DNA sliding clamp, exonuclease and tau. *eLife* **2015**, *4*, No. e11134.
(44) (a) Evans, R. J.; Davies, D. R.; Bullard, J. M.; Christensen, J.; Green, L. S.; Guiles, J. W.; Pata, J. D.; Ribble, W. K.; Janjic, N.; Jarvis, T. C. Structure of PolC reveals unique DNA binding and fidelity determinants. *Proc. Natl. Acad. Sci. U.S.A.* **2008**, *105*, 20695−20700. (b) Wing, R. A.; Bailey, S.; Steitz, T. A. Insights into the replisome from the structure of a ternary complex of the DNA polymerase III alpha-subunit. *J. Mol. Biol.* **2008**, *382*, 859−869.
(45) Brundret, K. M.; Dalziel, W.; Hesp, B.; Jarvis, J. A. J.; Neidle, S. X-Ray crystallographic determination of the structure of the antibiotic aphidicolin: a tetracyclic diterpenoid containing a new ring system. *J. Chem. Soc., Chem. Commun.* **1972**, 1027−1028.
(46) Inoue, R.; Kaito, C.; Tanabe, M.; Kamura, K.; Akimitsu, N.; Sekimizu, K. Genetic identification of two distinct DNA polymerases, DnaE and PolC, that are essential for chromosomal DNA replication in Staphylococcus aureus. *Mol. Genet. Genomics* **2001**, *266*, 564−571.
(47) Sinha, K. M.; Unciuleac, M. C.; Glickman, M. S.; Shuman, S. AdnAB: a new DSB-resecting motor-nuclease from mycobacteria. *Genes Dev.* **2009**, *23*, 1423−1437.
(48) Chauhan, A.; Lofton, H.; Maloney, E.; Moore, J.; Fol, M.; Madiraju, M. V.; Rajagopalan, M. Interference of *Mycobacterium tuberculosis* cell division by Rv2719c, a cell wall hydrolase. *Mol. Microbiol.* **2006**, *62*, 132−147.
(49) Bush, N. G.; Diez-Santos, I.; Abbott, L. R.; Maxwell, A. Quinolones: Mechanism, lethality and their contributions to antibiotic resistance. *Molecules* **2020**, *25*, 5662.
(50) Gillespie, S. H.; Basu, S.; Dickens, A. L.; O'Sullivan, D. M.; McHugh, T. D. Effect of subinhibitory concentrations of ciprofloxacin on Mycobacterium fortuitum mutation rates. *J. Antimicrob. Chemother.* **2005**, *56*, 344−348.
(51) Gupta, S.; Banerjee, S. K.; Chatterjee, A.; Sharma, A. K.; Kundu, M.; Basu, J. Essential protein SepF of mycobacteria interacts with FtsZ and MurG to regulate cell growth and division. *Microbiology* **2015**, *161*, 1627−1638.
(52) Bush, M. J. The actinobacterial WhiB-like (Wbl) family of transcription factors. *Mol. Microbiol.* **2018**, *110*, 663−676.
(53) Adefisayo, O. O.; Dupuy, P.; Nautiyal, A.; Bean, J. M.; Glickman, M. S. Division of labor between SOS and PafBC in mycobacterial DNA repair and mutagenesis. *Nucleic Acids Res.* **2021**, *49*, 12805−12819.
(54) Burby, P. E.; Simmons, L. A. Regulation of cell division in bacteria by monitoring genome integrity and DNA replication status. *J. Bacteriol.* **2020**, *202*, No. e00408.
(55) Jackson, M.; Raynaud, C.; Lanéelle, M. A.; Guilhot, C.; Laurent-Winter, C.; Ensergueix, D.; Gicquel, B.; Daffé, M. Inactivation of the antigen 85C gene profoundly affects the mycolate content and alters the permeability of the *Mycobacterium tuberculosis* cell envelope. *Mol. Microbiol.* **1999**, *31*, 1573−1587.
(56) Ioerger, T. R.; Feng, Y.; Ganesula, K.; Chen, X.; Dobos, K. M.; Fortune, S.; Jacobs, W. R., Jr; Mizrahi, V.; Parish, T.; Rubin, E.; Sassetti, C.; Sacchettini, J. C. Variation among genome sequences of H37Rv strains of *Mycobacterium tuberculosis* from multiple laboratories. *J. Bacteriol.* **2010**, *192*, 3645−3653.
(57) Snapper, S. B.; Melton, R. E.; Mustafa, S.; Kieser, T.; Jacobs, W. R., Jr. Isolation and characterization of efficient plasmid transformation mutants of *Mycobacterium smegmatis*. *Mol. Microbiol.* **1990**, *4*, 1911−1919.
(58) Shamputa, I. C.; Lee, J.; Allix-Beguec, C.; Cho, E. J.; Lee, J. I.; Rajan, V.; Lee, E. G.; Min, J. H.; Carroll, M. W.; Goldfeder, L. C.; Kim, J. H.; Kang, H. S.; Hwang, S.; Eum, S. Y.; Park, S. K.; Lee, H.; Supply, P.; Cho, S. N.; Via, L. E.; Barry, C. E., 3rd Genetic diversity of *Mycobacterium tuberculosis* isolates from a tertiary care tuberculosis hospital in South Korea. *J. Clin. Microbiol.* **2010**, *48*, 387−394.
(59) Abrahams, G. L.; Kumar, A.; Savvi, S.; Hung, A. W.; Wen, S.; Abell, C.; Barry, C. E., 3rd; Sherman, D. R.; Boshoff, H. I.; Mizrahi, V. Pathway-selective sensitization of *Mycobacterium tuberculosis* for target-based whole-cell screening. *Chem. Biol.* **2012**, *19*, 844−854.
(60) Valway, S. E.; Sanchez, M. P.; Shinnick, T. F.; Orme, I.; Agerton, T.; Hoy, D.; Jones, J. S.; Westmoreland, H.; Onorato, I. M. An outbreak involving extensive transmission of a virulent strain of *Mycobacterium tuberculosis*. *N. Engl. J. Med.* **1998**, *338*, 633−639.
(61) Manca, C.; Tsenova, L.; Bergtold, A.; Freeman, S.; Tovey, M.; Musser, J. M.; Barry, C. E., 3rd; Freedman, V. H.; Kaplan, G. Virulence of a *Mycobacterium tuberculosis* clinical isolate in mice is determined by failure to induce Th1 type immunity and is associated with induction of IFN-alpha /beta. *Proc. Natl. Acad. Sci. U.S.A.* **2001**, *98*, 5752−5757.
(62) Barrow, E. W.; Westbrook, L.; Bansal, N.; Suling, W. J.; Maddry, J. A.; Parker, W. B.; Barrow, W. W. Antimycobacterial activity of 2-methyl-adenosine. *J. Antimicrob. Chemother.* **2003**, *52*, 801−808.

https://doi.org/10.1021/acsinfecdis.1c00643
ACS Infect. Dis. 2022, 8, 612−625

(63) Cotsonas King, A.; Wu, L. Macromolecular synthesis and membrane perturbation assays for mechanisms of action studies of antimicrobial agents. *Curr. Protoc. Pharmacol.* **2009**, *47*, 13A-7.
(64) Schindelin, J.; Arganda-Carreras, I.; Frise, E.; Kaynig, V.; Longair, M.; Pietzsch, T.; Preibisch, S.; Rueden, C.; Saalfeld, S.; Schmid, B.; Tinevez, J.-Y.; White, D. J.; Hartenstein, V.; Eliceiri, K.; Tomancak, P.; Cardona, A. Fiji: an open-source platform for biological-image analysis. *Nat. Methods* **2012**, *9*, 676−682.
(65) Ducret, A.; Quardokus, E. M.; Brun, Y. V. MicrobeJ, a tool for high throughput bacterial cell detection and quantitative analysis. *Nat. Microbiol.* **2016**, *1*, 16077.
(66) R Core Team. *R: A Language and Environment for Statistical Computing*; R Foundation for Statistical Computing, RStudio Team. *RStudio: Integrated development for R; PBC*, 2020.
(67) FastQC: A quality control tool for high throughput sequence data. 2010, http://www.bioinformatics.babraham.ac.uk/projects/fastqc/.
(68) Wang, L.; Nie, J.; Sicotte, H.; Li, Y.; Eckel-Passow, J. E.; Dasari, S.; Vedell, P. T.; Barman, P.; Wang, L.; Weinshiboum, R.; Jen, J.; Huang, H.; Kohli, M.; Kocher, J.-P. A. Measure transcript integrity using RNA-seq data. *BMC Bioinf.* **2016**, *17*, No. 58.
(69) Sayols, S.; Scherzinger, D.; Klein, H. dupRadar: a Bioconductor package for the assessment of PCR artifacts in RNA-Seq data. *BMC Bioinf.* **2016**, *17*, No. 428.
(70) Ewels, P.; Magnusson, M.; Lundin, S.; Käller, M. MultiQC: summarize analysis results for multiple tools and samples in a single report. *Bioinformatics* **2016**, *32*, 3047−3048.
(71) Patro, R.; Duggal, G.; Love, M. I.; Irizarry, R. A.; Kingsford, C. Salmon provides fast and bias-aware quantification of transcript expression. *Nat. Methods* **2017**, *14*, 417−419.
(72) Love, M. I.; Huber, W.; Anders, S. Moderated estimation of fold change and dispersion for RNA-seq data with DESeq. 2. *Genome Biol.* **2014**, *15*, No. 550.
(73) Szklarczyk, D.; Gable, A. L.; Lyon, D.; Junge, A.; Wyder, S.; Huerta-Cepas, J.; Simonovic, M.; Doncheva, N. T.; Morris, J. H.; Bork, P.; Jensen, L. J.; von Mering, C. STRING v11: protein−protein association networks with increased coverage, supporting functional discovery in genome-wide experimental datasets. *Nucleic Acids Res.* **2019**, *47*, D607−D613.
(74) Kolbe, K.; Bell, A. C.; Prosser, G. A.; Assmann, M.; Yang, H.-J.; Forbes, H. E.; Gallucci, S.; Mayer-Barber, K. D.; Boshoff, H. I.; Barry, C. E., 3rd Development and optimization of chromosomally-integrated fluorescent *Mycobacterium tuberculosis* reporter constructs. *Front. Microbiol.* **2020**, *11*, No. 591866.
(75) Toste Rêgo, A.; Holding, A. N.; Kent, H.; Lamers, M. H. Architecture of the Pol III-clamp-exonuclease complex reveals key roles of the exonuclease subunit in processive DNA synthesis and repair. *EMBO J.* **2013**, *32*, 1334−1343.
(76) Zivanov, J.; Nakane, T.; Forsberg, B. O.; Kimanius, D.; Hagen, W. J.; Lindahl, E.; Scheres, S. H. New tools for automated high-resolution cryo-EM structure determination in RELION-3. *eLife* **2018**, *7*, No. e42166.
(77) Zhang, K. Gctf: Real-time CTF determination and correction. *J. Struct. Biol.* **2016**, *193*, 1−12.
(78) Subramaniya, S. R. M. V.; Terashi, G.; Kihara, D. Super-Resolution cryo-EM Maps with 3D deep generative networks. *bioRxiv* **2021**, DOI: 10.1101/2021.01.12.426430.
(79) Emsley, P.; Lohkamp, B.; Scott, W. G.; Cowtan, K. Features and development of Coot. *Acta Crystallogr., Sect. D: Biol. Crystallogr.* **2010**, *66*, 486−501.
(80) Murshudov, G. N.; Skubak, P.; Lebedev, A. A.; Pannu, N. S.; Steiner, R. A.; Nicholls, R. A.; Winn, M. D.; Long, F.; Vagin, A. A. REFMACS for the refinement of macromolecular crystal structures. *Acta Crystallogr., Sect. D: Biol. Crystallogr.* **2011**, *67*, 355−367.
(81) Nicholls, R. A.; Tykac, M.; Kovalevskiy, O.; Murshudov, G. N. Current approaches for the fitting and refinement of atomic models into cryo-EM maps using CCP-EM. *Acta Crystallogr., Sect. D: Struct. Biol.* **2018**, *74*, 492−505.
(82) Liebschner, D.; Afonine, P. V.; Baker, M. L.; Bunkoczi, G.; Chen, V. B.; Croll, T. I.; Hintze, B.; Hung, L. W.; Jain, S.; McCoy, A. J.; Moriarty, N. W.; Oeffner, R. D.; Poon, B. K.; Prisant, M. G.; Read, R. J.; Richardson, J. S.; Richardson, D. C.; Sammito, M. D.; Sobolev, O. V.; Stockwell, D. H.; Terwilliger, T. C.; Urzhumtsev, A. G.; Videau, L. L.; Williams, C. J.; Adams, P. D. Macromolecular structure determination using X-rays, neutrons and electrons: recent developments in Phenix. *Acta Crystallogr., Sect. D: Struct. Biol.* **2019**, *75*, 861−877.